MEAN FIELD THEORY FOR STRUCTURAL PHASE TRANSITION IN Y-Ba-Cu-O

A thesis submitted to the School of Graduate Studies
Addis Ababa University

In partial Fulfillment of the Requirements for the
Degree of Master of Science in Physics

By

Ashenafi Weldemariam

Addis Ababa, Ethiopia
July 2007

ADDIS ABABA UNIVERSITY
DEPARTMENT OF
PHYSICS

The undersigned hereby certify that they have read and recommend to the Faculty of Graduate Studies for acceptance a thesis entitled "**MEAN FIELD THEORY FOR STRUCTURAL PHASE TRANSITION IN Y-Ba-Cu-O**" by **Ashenafi Weldemariam** in partial fulfillment of the requirements for the degree of **Master of Science**.

Advisor: _____
Dr. Sib Krishna Ghoshal

Examiner: _____
Prof. Singh P.

Examiner: _____
Dr. Tewari H.S.

This work is dedicate

To My Father Weldemariam Gebregiorgis

1944-1987 E.C.

Table of Contents

List of Tables

List of Figures

Abstract

The spring-defect-model has been developed earlier for describing the structural phase transition in YBCO (from tetragonal to orthorhombic at ∼900K) in high $T_c(\lesssim 92K)$ superconductor is now casted into effective strain-strain interaction Hamiltonian. In this model the connection between elastic distortion and oxygen ordering is described using mean field theory. The lattice static of the Cu-O basal plane is treated in the harmonic approximation in which oxygen and vacancy are modeled via pseudo spin $\hat{S} = \pm 1$. The strain model is suitable for describing paraelastic (tetragonal) to ferroelastic (orthorhombic) transition in YBCO. The orthorhombic phase is known to be ferroelastic and it develop spontaneous strain due to oxygen ordering in one direction of lattice.

We present the results for ferroelastic order parameter, static compliance, frequency dependent compliance and internal friction in terms of all the basic parameter like spring constants K, K' distortion parameter α, lattice constants a_0 of the model. The signature of phase transition is occurred through ferroelastic and anelastic relaxation from mean field approximation of the strain-strain model under the influence of an external in homogeneous stress. These are very important results as far as formation of tweed textures and mechanical behavior in YBCO is concerned. The model is 2D as our focus is on the Cu-O basal plane of 3D structures.

Our main aim is to describe the statics and kinetics of the ferroelastic transition in YBCO

Acknowledgements

The completion of this work would not be possible without the support of Dr. Sib Krishna Ghoshal, my family and my friends. First, I would like to thank my advisor, Dr. Sib Krishna Ghoshal certainly, his supervision, advice and patience were very important throughout these year. I also would like to thank all the people that I have met during the last two years at AAU.

The last two year at AAU would not have been so easy it was not by the group of people I met at the New Life Campus Fellowship, indeed a church for the new generation. These dissertation would not be complete without mention all friends that were close to me during the past year. I could not be thankful enough for the support of my family. This accomplishment would not be the same if I could not share it with my family. I am thankful for all the support I received from them.

Finally, I sincerely thank all my colleagues specially Hag, Shiba, berbatove, fanteshe etc. and the Ministry of Education for all the support I have received. Last but in no way least the biggest thanks to my be loving Mama and my brothers Dawit, Mike and my younger brother Haftshe, my sisters Ferita, Samere, netse, sene and my aunt with her family for their unlimited support during my M.Sc. studies.

Ethiopia, Addis Ababa
July 25, 2007

Ashenafi Weldemariam
E-mail: $ashenafi\_2010@yahoo.com$

Introduction

There are few absolute in physics

> *Most concepts and ideas are approximations, often excellent, but rarely something, you would claim to be absolutely exact. However, the state of absolute zero resistance does exist*

i.e., superconductivity.

The discovery of high-T_c superconducting materials by Bednorz and Müller in 1986 [1] set into motion an unprecedented worldwide outburst of research into superconductivity. Soon after Kamerlingh Onnes discovered superconductivity, scientists began dreaming up practical applications for this strange new phenomenon at room temperature. There are numerous applications for superconductors such as levitating trains, smaller cheaper medical imaging equipment, power line conductors, super fast computers, floating cars, electromagnetic spacecraft launching devices, high Tesla electromagnets, magicians equipment, floating furniture, SQUIDS, non-contact bearings, etc. But the really exciting thing is that the best applications have not even been thought of yet.

Superconductivity was soon discovered in other cuprates, after the discovery of the first high-T_c superconductor including $YBa_2Cu_3O_{7-\delta}$ (YBCO) in 1987 [2]. Optimally

doped, YBCO has a $T_c \approx 92K$. In addition, to the high transition temperatures, the cuprate superconductors exhibit many unusual features for superconducting materials, including very large spatial anisotropy, extremely small coherence lengths, and close proximity to magnetically ordered (antiferromagnetic) phases.

The layered perovskite cuprate materials are a unique class of superconductors with unusual normal-state and superconducting properties. The common physics to all these materials is that of the underlying CuO_2 planes. The high-T_c superconductor $YBa_2Cu_3O_{7-\delta}$ (YBCO) has a large potential in technological applications such as magnetic shielding devices, medical imaging systems, superconducting quantum interference devices (SQUIDS), infrared sensors, analog signal processing devices, and microwave devices. Over the last few years the experimental and theoretical study of the high temperature superconducting (HTSC) cuprates remains one of the leading issues in the physics of condensed matter [3].

In this study, we are going to Model the Cu-O basal plane of $YBa_2Cu_3O_{7-\delta}$ as a 2D-Ising system in which the copper atoms are assumed to be connected by spring constants 'K' along the chain and 'K'' along the diagonal. Then we find the Hamiltonian which is the defect-defect interaction. The focus of this thesis is on to find whether there is a phase transition in YBCO and to find the order parameter and the compliance of YBCO and analysis of the results.

The aim of this work is to use mean field approximation (MFA) to the Hamiltonian to find the order parameter and the compliance of YBCO. A many-body system with interactions is generally very difficult to solve exactly. The great difficulty when computing the partition function of the system is the treatment of combinatorics

generated by the interaction terms in the Hamiltonian when summing over all states. The goal of mean field theory is to resolve these combinatorial problems. The main idea of MFT is to replace all interactions to any one body with an average or effective interaction. This reduces any multi-body problem into an effective one-body problem i.e., is to focus on one particle and assume that the most important contribution to the interactions of such particle with its neighboring particles is determined by the mean field due to the neighboring particles. In field theory, the Hamiltonian may be expanded in terms of the magnitude of fluctuations around the mean of the field. In this context, MFT can be viewed as the "zeroth-order" expansion of the Hamiltonian in fluctuations i.e., MFT system has no fluctuations.

The thesis basically consists of three main parts. In the first chapter, we find some background information about the physical properties of YBCO and and genarally about superconductors. In the second chapter the model Hamiltonian and the static effects from mean field treatment, and using the MFA we will find the static compliance of YBCO. In the third chapter we will see kinetics using mean field theory and anelastic relaxation the response of the system at the onset of structural phase transition. Finally, we will discuss the results.

Chapter 1

Superconductivity

The field of superconductivity, once a mere laboratory curiosity, has moved into the realm of applied science in recent years. Even more applications may become possible because of the discovery of ceramic superconductors, which operate at comparatively "high" temperatures. One of such high T_c ceramic called $YBCO$ and its structural transition is of our interest in the present thesis. However, before we proceed to discuss our problem it is customary to give a short introduction on superconductivity.

1.1 Introduction

Room temperature superconductors (or even materials that will superconductor via Freon cooling) are one of the next great technological leaps awaiting mankind. Even liquid N_2 cooled superconductors that can easily be formed into flexible wires would be a great leap. If higher temperature superconductors (room temperature) can be developed, it has the potential to change the world into the science fiction representation we often see in the movies (floating cars, trains, furniture, etc).

High temperature superconductors (HTS) and their characteristics are fascinating topics. In this chapter, we will introduce how superconductors devolved from the begin, the fundamental properties of superconductors, the basics of high temperature superconductors particularly YBCO, the Meissner effect, the zero resistance effect, and in the last section we will see some applications of superconductors.

1.2 History

Superconductivity was discovered by Dutch physicist Heike Kamerlingh Onnes in Holland in 1911, as a result of his investigations leading to the liquefaction of helium gas. Two years later, he got the Nobel Prize for his great contribution [3]. The Dutch physicist known for his research into phenomena at extremely low temperature. In 1908, Onnes had become the first person to liquefy helium. He was investigated the electrical properties of various substances at liquid helium temperature (4.2 K) when he noticed that the resistivity of mercury dropped abruptly at 4.2 K to a value below the resolution of his instruments. For obvious technological reasons, the search continued for materials which could superconduct at higher temperatures. Despite much work, for decades the highest T_c's belonged to Nb_3Sn (18K) then Nb_3Ge (23K), and the field was considered by many to be at a dead end. A history of the increase in record T_c is shown in Fig.(1.1). During the 75 years that followed, great studies were made in the understanding of how superconductors work. Over that time, various alloys were found that show superconductivity at somewhat higher temperatures. In 1933, W.Meissner and R.Oschenfeld discovered that a metal cooled into the superconducting state in a weak magnetic field expels the magnetic field from

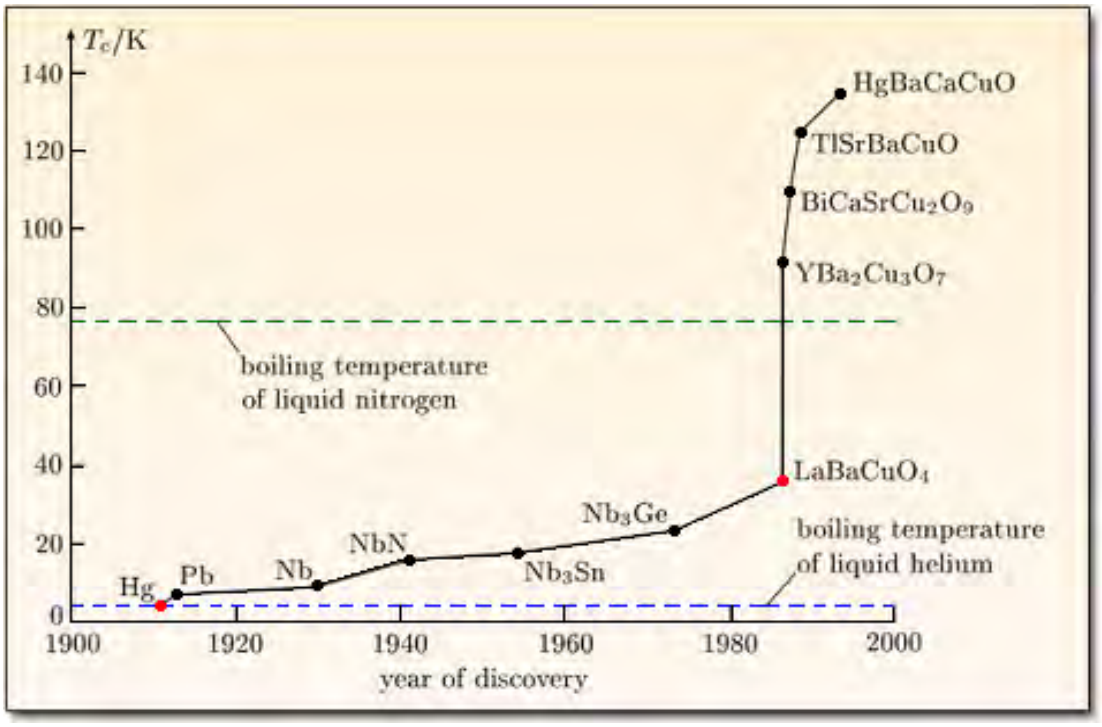

Figure 1.1: *Discovery of materials with successively higher T_c's over the last century. (Points circled in red garnered a Nobel Prize for their discoverers: Kamerlingh-Onnes in 1913 and Bednorz and Müller in 1987.)*

its interior. In 1947, the Russian physicist V. Arkadiev first performed the now-classic experiment of using this expulsion of a magnetic field to levitate a small bar magnet above the surface of a superconductor. Today, with liquid nitrogen and modern high-temperature superconductors, Arkadiev's levitation is a common trick in the physics classroom [4].

The first widely-accepted theoretical understanding of superconductivity was advanced in 1957 by American physicists John Bardeen, Leon Cooper, and John Schrieffer. Their Theories of Superconductivity became know as the *BCS* theory - derived

from the first letter of each man's last name and won them a Nobel prize in 1972. The mathematically-complex *BCS* theory explained superconductivity at temperatures close to absolute zero for elements and simple alloys. However, at higher temperatures and with different superconductor systems, the *BCS* theory has subsequently become inadequate to fully explain how superconductivity is occurring. Another significant theoretical advancement came in 1962 when Brian D. Josephson, a graduate student at Cambridge University, predicted that electrical current would flow between two superconducting materials even when they are separated by a non-superconductor or insulator. His prediction was later confirmed and won him a share of the 1973 Nobel Prize in Physics. This tunneling phenomenon is today known as the *"Josephson effect"* and has been applied to electronic devices such as the SQUID, an instrument capable of detecting even the weakest magnetic fields [3].

Advances in superconductivity continued to proceed slowly. During the first 75 years of superconductivity research, the critical temperature (the temperature below which superconductivity is present) was raised by less than 20 degrees. In 1973, a niobium alloy was produced with a critical temperature of 23.2 K. Finally, in January of 1987, one of those rare authentic technological breakthroughs occurred when researchers at the University of Alabama at Huntsville and at the University of Houston produced ceramic superconductors with a critical temperature above the temperature of liquid nitrogen [5].

The history of high-temperature superconductivity as a field distinct from ordinary superconductivity is very brief. It began in late 1986 when news spread that J.Geoorge

Bednorz and K.Alex Müller [1] of the IBM research laboratory in Zurich, Switzerland, had reported the observation of superconductivity in Lanthanum Copper Oxides doped with Barium or Strontium at temperature upto 38K. This caused tremendous excitement because 38K was above the ceiling of 30K for superconductivity that had been theoretically predicted almost 20 years earlier and which had become an unquestioned belief among scientists and engineers interested in superconductivity [6]. Once the barrier was broken, scientists set into motion an unprecedented worldwide outburst of research into superconductivity. Superconductivity was soon discovered in other cuprates, including $YBa_2Cu_3O_{7-\delta}$(YBCO) in 1987 [2]. Optimally doped, YBCO has a T_c=92 K (see fig.(1.2)). In addition to the high transition temperatures, the cuprate superconductors exhibit many unusual features for superconducting materials, including very large spatial anisotropy, extremely small coherence lengths, and close proximity to magnetically ordered (antiferromagnetic) phases.

The high-T_c superconductors are interesting to study for several reasons. Theoretically, the reason these materials have a superconducting state is unclear, as is the exact mechanism for superconductivity in the materials. This is partially due to their complex structure, both electronic and physical. Developing a full understanding of superconductivity in the high-T_c regime is an important problem in solid-state physics. In addition, the high-T_c superconductors have a vast and varied potential for applied use. Superconducting devices have many well-developed uses, with SQUIDs and tunnel junctions being some of the most well known. Materials that have a T_c greater than 77 K can be used to make these devices work at liquid nitrogen temperatures. This makes these devices much cheaper and easier to use than devices requiring liquid helium to function, which is a major advantage.

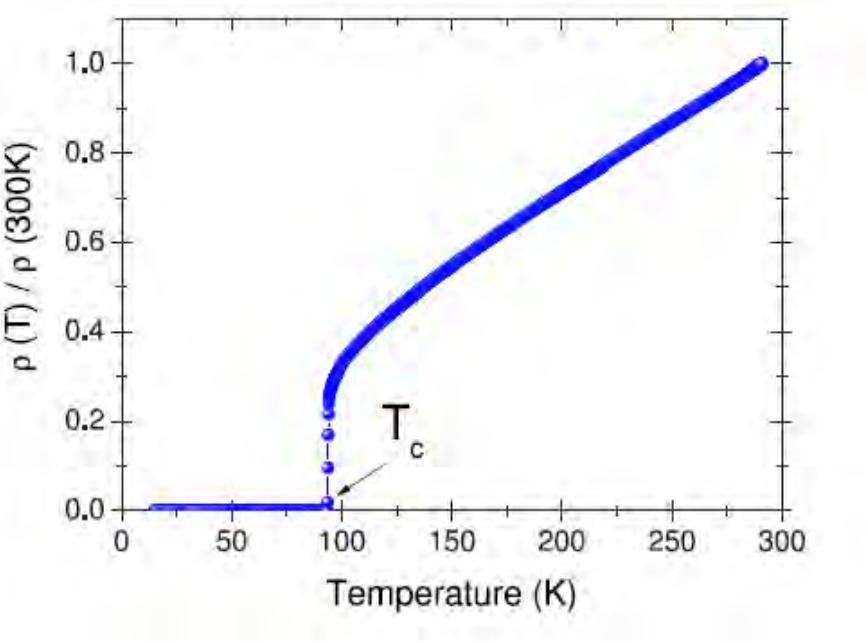

Figure 1.2: *Temperature dependence of the resistivity of high-T_c superconductor $YBa_2Cu_3O_{7-\delta}$*

The phenomenon of superconductivity has had a tremendous impact on the advancement of technology in many fields including medicine, electronics, motors, power, transportation and communication. Accordingly, the call to develop superconducting materials is strong and will remain so as the technology improves and becomes less expensive. Discovering or developing a superconducting material with a room temperature superconducting state is the ultimate challenge in superconductivity, but with the uncertainty of this ever being achieved, the current focus of much of the research, development and commercialization of superconductors is on YBCO.

From 1911, when superconductivity was discovered, until 1986, as shown in Tab.(1.1) when a Lanthanum Cuprate ceramic material was found to be superconductive, there

Year		Material	$T_c(K)$
1964		NbO	1
1964		TiO	2
1964	doped	$SrTiO_{3-x}$	0.7
1965	bronzes	K_xWO_3	6
1966	bronzes	K_xMoO_3	4
1969	bronzes	K_xReO_3	4
1974		$LiTi_2O_4$	13
1975		$Ba(Pb,Bi)O_3$	13
1986		$La_{1.85}Sr_{0.15}CuO_4$	38
1887		$YBa_2Cu_3O_{7-\delta}$	93
1988		$Tl_2Ba_2Ca_2Cu_3O_{10}$	125
1994		$HgBa_2Ca_2Cu_3O_{8+\delta}$	133

Table 1.1: *Year of discovery and critical temperature T_c of some oxide superconductors.*

were no ceramic materials known to exhibit superconductivity. Even with the breakthrough of the first ceramic superconductor, the temperature at which this phenomenon occurred was still extremely low. The discovery of a YBCO superconducting material in 1987 brought about a great excitement within the scientific community. The idea that a material can conduct electricity free of resistance, at temperatures above 77 K, the temperature at which nitrogen liquefies, opened up the possibility for numerous advancements for electronic and wire technologies. The development of such devices, however, turned out to be a very difficult task. Among the major barriers are the inherent brittleness of YBCO and the high processing temperature required to produce the superconducting phase.

In order to comprehend the nature of YBCO superconductors and the obstacles they face in application, it is essential to have an understanding of the three main parameters that characterize superconductivity. The first of which, the critical temperature

or transition temperature, indicates the temperature at which the material switches between the normally conductive state and the superconductive state. The second parameter, the critical magnetic field, indicates the maximum strength of the magnetic field that can be endured without completely destroying the superconducting state. Finally, the critical current density is the third parameter that characterizes superconductors, and it indicates the maximum amount of current that can flow through an area of the superconductor [7]. These three parameters are the fundamental characteristics of YBCO with respect to its superconducting capabilities. To improve these and other properties, various processing techniques have been explored and used. Producing YBCO in different forms is essential in order to fabricate YBCO materials with the necessary properties for the desired applications. Achieving this, though, is not always a simple matter.

Unfortunately, the high-temperature superconductors have two major drawbacks: they are very brittle (like most ceramics), they do not carry enough current to be very useful [6]. The brittleness and the development of a continuous processing method are the major issues for the development of YBCO superconducting wires. YBCO depositions onto nickel based substrates have been successful to increase the ductility of the wire, but the lack of a continuous processing method has limited the length of YBCO wires that can be produced. Bulk YBCO superconductors are primarily used in levitation applications, where they levitate a permanent magnet to perform some function. Thin and thick films of YBCO are generally used for electronic and wire technologies.

The first application of YBCO superconductors was realized in bulk form for magnetic devices. Superconducting magnets are used in medical as well as energy storage devices. Magnetic resonance imaging (MRI) devices had been around before the discovery of superconducting YBCO, but the newer high temperature superconducting material reduced costs compared to earlier technology. While YBCO superconductors are suitable materials for many applications, complex designs and high operating costs of the cooling systems required for proper superconductor performance are the primary obstacles preventing broader implementation of systems utilizing YBCO superconductors.

1.3 What is a Superconductor?

Superconducting materials have two fundamental properties:

- No dc-resistivity ($\rho = 0$ for all T $\leq T_c$): Zero resistivity $\rho = 0$, i.e. infinite conductivity, is observed in a superconductor at all temperatures below the critical temperature T_c, as depicted in Fig.(1.2). However, if the passing current is higher than the critical current j_c , superconductivity disappears. *Why is the resistivity of a superconductor zero?* If a superconducting metal like Al or Hg is cooled below the critical temperature T_c, the gas of repulsive individual electrons that characterizes the normal state transform itself into a different type of fluid, a quantum fluid of highly correlated pairs of electrons. A conduction electron of a given momentum and spin gets weakly coupled with another electron of the opposite momentum and spin. These pairs are called Cooper pairs. The coupling energy is provided by lattice elastic waves, called phonons. The

behavior of such a fluid of correlated Cooper pairs is different from the normal electron gas. They all move in a single coherent motion. A local perturbation, like an impurity, which in the normal state would scatter conduction electrons (and cause resistivity), can not do so in the superconducting state without immediately affecting the Cooper pairs that participate in the collective superconducting state. Once this collective, highly coordinated, state of coherent super-electrons (Cooper pairs) is set into motion (like the supercurrent induced around the loop), its flow is without any dissipation. There is no scattering of individual pairs of the coherent fluid, and therefore no resistivity.

- No magnetic induction (B = 0 inside the superconductor): In magnetic fields lower the critical field B_c the magnetic inductance becomes zero inside the superconductor when it is cooled below T_c. The magnetic flux is expelled from the interior of the superconductor (see Fig.1.3). This effect is called the Meissner-

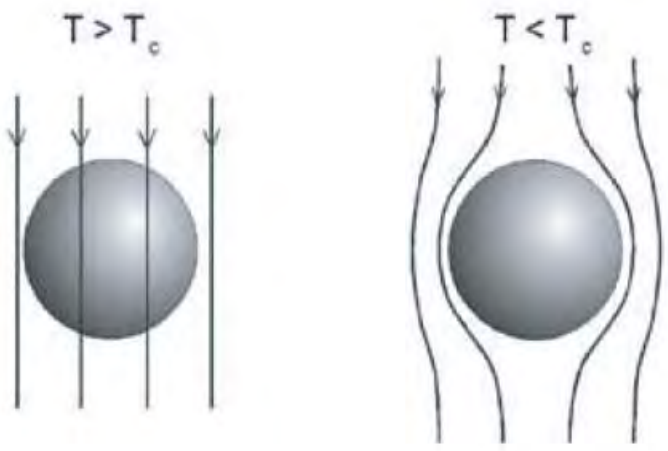

Figure 1.3: *Expulsion of a weak external magnetic field from the interior of the superconducting sample.*

Ochsenfeld effect after its discoverers [8]. To test whatever a material is superconducting both properties $\rho = 0$ and B = 0 must be present simultaneously.

1.4 Superconductivity in $YBa_2Cu_3O_{7-\delta}$(YBCO)

The high-temperature superconductors known as perovskites are a mixture of metal oxides, which display the mechanical and physical properties of ceramics. $YBa_2Cu_3O_{7-\delta}$ (YBCO) is a very common Type II superconductor. A key element to the behavior of these materials is the presence of planes containing copper and oxygen atoms chemically bonded to each other. The special nature of the Cu-O chemical bond permits materials to conduct electricity very well in some directions.

Most ceramic materials are considered good electrical insulators. YBCO compounds, also known as 1-2-3 compounds, are very sensitive to oxygen content. They change from semiconductors at $YBa_2Cu_3O_{6.5}$ to superconductors at $YBa_2Cu_3O_{7-\delta}$ with out losing their crystalline structure. The high sensitivity of superconductors to oxygen content is due to the apparent ease to which oxygen can move in and out of the molecular lattice. According to the formula, $YBa_2Cu_3O_7$, the metals are in a mole ratio of 1-2-3.

Among the high T_c superconductors, YBCO was one of the first synthesized, and is still one of the more widely studied. All high-T_c superconductors have a layered structure, in which the presence of CuO_2 layers plays a determinant role in their superconducting character. The carriers only move along these planes, while the other components act as charge reservoirs that regulate the charge density in the

CuO_2 planes. In the particular case of YBCO, each unit cell contains two CuO_2 planes, separated by a plane of ytrium atoms, and sandwiched by two Ba-O layers, as shown in the Fig.(1.5).

The compound can present two possible symmetries, tetragonal or orthorhombic, depending on the amount and distribution of oxygen in the final Cu-O layers which close the cell. For low oxygen concentration ($\delta \approx 1$), oxygen atoms are randomly

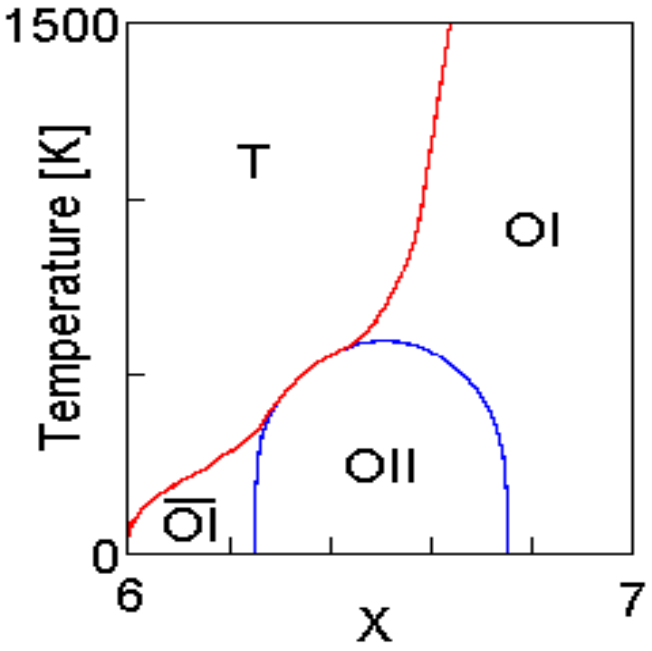

Figure 1.4: *Phase diagram calculated theoretically. T labels the tetragonal Phase, OI, OII etc. label the orthorhombic phases.*

disperse in their four possible sites between Cu in the top and bottom planes, leading to a tetragonal structure (scheme (a) in the figure(1.5)). However, for δ close to zero, oxygen atoms are ordered occupying only inter-Cu sites along the b-axis of these

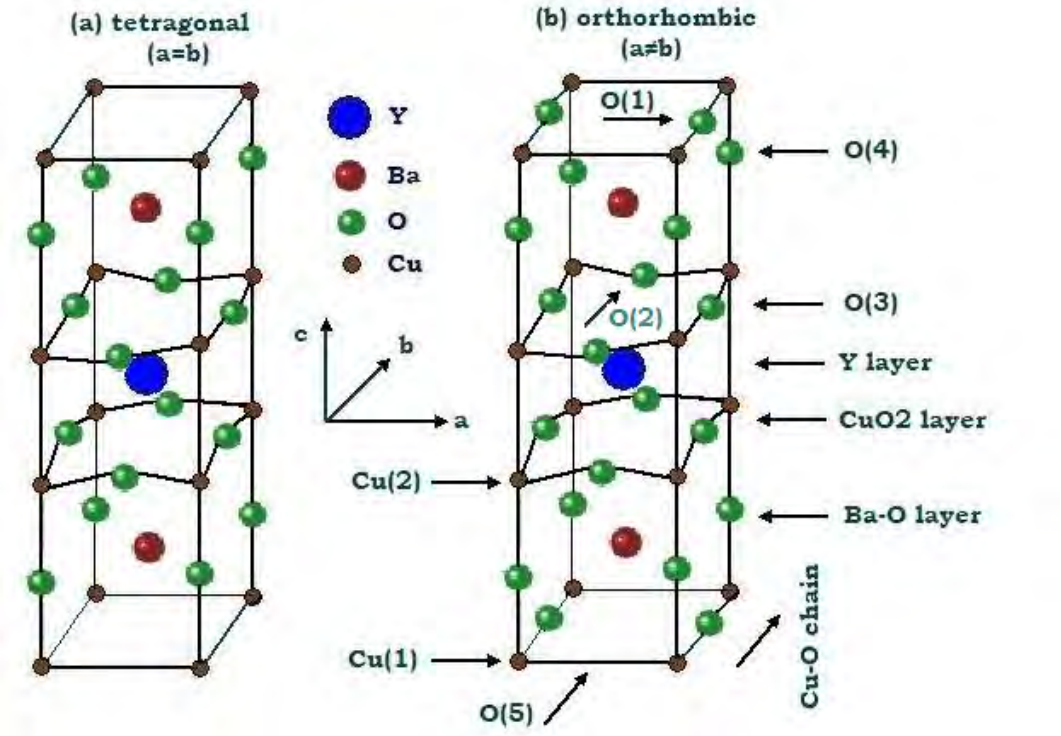

Figure 1.5: *Schematic diagrams of* $YBa_2Cu_3O_6$ *(left) an insulator and* $YBa_2Cu_3O_7$ *(right) a superconducting oxide.*

planes, and this leads to a orthorhombic structure (scheme (b) in the figure(1.5)). In this case, the Cu-O atoms form chains more than planes, and so they are referred this second structure is the only one superconducting. YBCO exists in a tetragonal (fig. (1.5)) and at least two orthorhombic phases (fig. (1.5, 1.4)) depending on x ($6 < x < 7$) and the temperature [9]. The phases differ in number and order of O atoms on interstitial sites in the Cu(1) plane. The several orthorhombic phases differ from each other in oxygen configuration superstructures.

The ceramic superconductors of greatest interest are very anisotopic; that is, their

properties are quite different in different crystalline directions [6]. Most of the processes to obtain YBCO samples result in poorly oxygenated, and then tetragonal, structures. In these cases, samples must be oxygenated to obtain the superconducting orthorhombic phase. In order to achieve a material with the optimum oxygen content (optimally doped), samples must be heated in flowing oxygen, at around 400-550 $^{\circ}C$, during a period which depends on the size of the sample. As the rest of high-T_c superconductors, YBCO is a type II superconductor. The flux of carriers along their CuO_2 layers causes a high anisotropy in these materials, whose properties are different in the ab-plane directions and the c-axis direction [10].

1.5 Applications of Superconductors

Existing applications in the high temperature range all relate to copper oxide superconductors, although high quality tapes and wires have been made from MgB_2, so there is a strong possibility that this material will also find its way into applications in the future. Low temperature (LTS) superconductors found their way into serious use in electromagnets and other applications in the 1960s. There were thus very high hopes for the high temperature (HTS) copper oxide superconductors from the time they were discovered in 1986 by Bednorz and Müller. This was because of the very much lower costs of refrigeration at liquid nitrogen temperature and because the mechanisms for this new type of superconductivity were not well understood, leading to hopes that it might be possible to find a room temperature superconductor. In reality, formidable materials science problems had to be solved, largely due to the ceramic, granular, anisotropic nature of the HTS materials. They are all very brittle and difficult to shape, and need to be formed at high temperatures in the presence of

oxygen [11].

There are numerous applications for superconductors such as levitating trains, smaller cheaper medical imaging equipment, power line conductors, super fast computers, floating cars, electromagnetic spacecraft launching devices, high Tesla electromagnets, magicians equipment, floating furniture, non-contact bearings, etc. But the really exciting thing is that the best applications have not even been thought of yet [12].

Soon after Kamerlingh Onnes discovered superconductivity, scientists began dreaming up practical applications for this strange new phenomenon. The recent discovery of high temperature superconductors brings us a giant step closer to the dream of early scientists. Applications currently being explored are mostly extensions of current technology used with the low temperature superconductors. Current applications of high temperature superconductors include; magnetic shielding devices, medical imaging systems, superconducting quantum interference devices (SQUIDS), infrared sensors, analog signal processing devices, and microwave devices. As our understanding of the properties of superconducting material increases, applications such as; power transmission, superconducting magnets in generators, energy storage devices, particle accelerators, levitated vehicle transportation, rotating machinery, and magnetic separators will become more practical.

The ability of superconductors to conduct electricity with zero resistance can be exploited in the use of electrical transmission lines. Currently, a substantial fraction of electricity is lost as heat through resistance associated with traditional conductors such as copper or aluminum. A large scale shift to superconductivity technology

depends on whether wires can be prepared from the brittle ceramics that retain their superconductivity at 77 K while supporting large current densities.

The field of electronics holds great promise for practical applications of superconductors. The miniaturization and increased speed of computer chips are limited by the generation of heat and the charging time of capacitors due to the resistance of the interconnecting metal films. The use of new superconductive films may result in more densely packed chips which could transmit information more rapidly by several orders of magnitude. Superconducting electronics have achieved impressive accomplishments in the field of digital electronics. Through the use of basic Josephson junctions scientists are able to make very sensitive microwave detectors, magnetometers, SQUIDs and very stable voltage sources.

The use of superconductors for transportation has already been established using liquid helium as a refrigerant. Prototype levitated trains have been constructed in Japan by using superconducting magnets.

Superconducting magnets are already crucial components of several technologies. Magnetic resonance imaging (MRI) is playing an ever increasing role in diagnostic medicine. The intense magnetic fields that are needed for these instruments are a perfect application of superconductors. Similarly, particle accelerators used in high-energy physics studies are very dependant on high-field superconducting magnets. The recent controversy surrounding the continued funding for the Superconducting Super Collider (SSC) illustrates the political ramifications of the applications of new technologies.

New applications of superconductors will increase with critical temperature. Liquid nitrogen based superconductors has provided industry more flexibility to utilize superconductivity as compared to liquid helium superconductors. The possible discovery of room temperature superconductors has the potential to bring superconducting devices into our every-day lives [13].

Since the last decade of 20^{th} century YBCO is a major focus of attention for various applied reason. As this system undergoes a phase transition (structural) from tetragonal to orthorhombic it enters into a new phase called ferroelastic (a spontaneous strain without external stress) [14] which is very useful for mechanical switches and tuned grating. However there is no systematic way of understanding these mechanical properties through microscopic modeling we would like to understand some of its mechanical properties at the onset of structural phase transition.

Chapter 2

Ferroelasticity In YBCO

In this chapter we are going to discus about ferroelasticity in $YBa_2Cu_3O_{7-\delta}$. YBCO is an oxidic ceramic, that has technical interest because of its superconducting and unusual mechanical properties. It is of tetragonal or orthorhombic structure (fig.1.5) depending on its oxygen content (usually x between 6 and 7) and temperature [9]. These two structures correspond to different oxygen configurations. The phase transitions between the structures are order-disorder processes due to diffusion jumps of the oxygen atoms in Cu-O planes.

The tetragonal-to-orthorhombic phase transition is interesting due to several reasons. It is ferroelastic, i.e. small stresses can cause huge strains (comparable to ferromagnetism or ferroelectricity) and develops spontaneous strain. Therefore YBCO can be used as a model system for ferroelastic phase transitions. In addition one can use the ferroelastic behaviour to prevent twinning during crystal growth or to countermand it subsequently. The ferroelasticity in YBCO is seen at the onset of structural phase transition from tetragonal to orthorhombic phase. The development of such atomic is reflected in ultrasonic attenuation and internal friction experiment.

2.1 Introduction

As mentioned in the first chapter, it is widely believed that superconductivity in YBCO is strongly linked with the ordering of oxygen atoms in the basal plane. The evidence for this comes from the variation of the superconducting transition temperature $T_c(\delta)$ with the stoichiometry δ of oxygen (see fig.2.1). As oxygen ordering

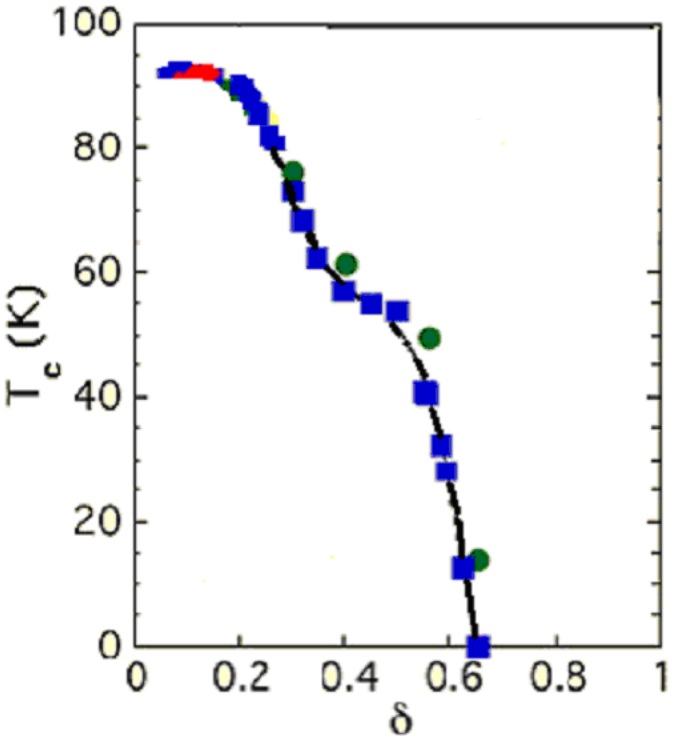

Figure 2.1: *Superconducting transition temperature-T_c vs. oxygen deficient. Two plateaus are evident, at T_c=90K and 60K.*

is also thought to give rise to the orthorhombicity of the crystal it is important to understand the mechanism of structural phase transition in YBCO. For $\delta = 0$ this transition occurs at around 900K when, on cooling the system goes from a tetragonal

($a = b \neq c$) to an orthorhombic ($a \neq b \neq c$) phase. In the tetragonal phase 50% of the available oxygen sites in the basal plane are occupied by oxygen at random in the interstitial positions while the rest are vacant. On the other hand, in the fully ordered orthorhombic phase, alternate Cu-O chains parallel to the b-axis are formed. As a result the lattice is stretched along the b-axis and remain unstretched along the a-axis leading to an orthorhombic distortion. This distortion makes the orthorhombic phase ferroelastic. It is therefore reasonable to construct a lattice-gas model comprising the

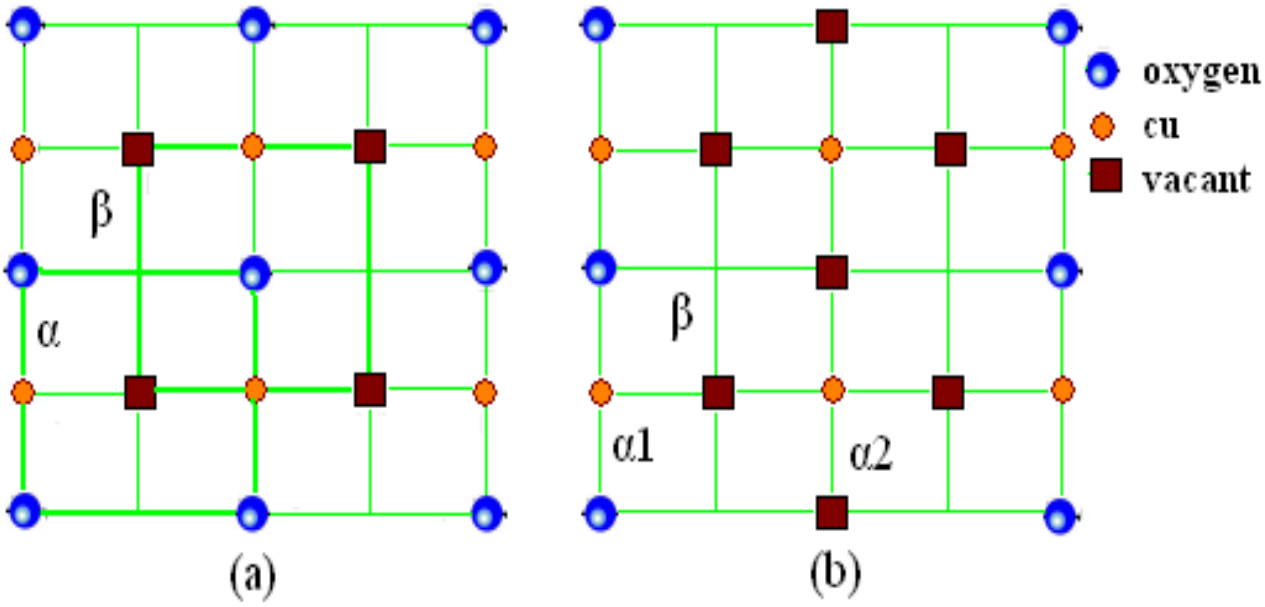

Figure 2.2: *Ground states in the Cu-O basal plane. (a) At $c_o = 0.5$ two sublattices α and β are present. (b) At $c_o = 0.25$ a cell-doubling phase gives rise to sublattices α_1, α_2, and β.*

oxygen-sites in the basal plane in which the presence of the oxygen atom in a given site is associated with an Ising-spin $\hat{S} = +1$ whereas a vacancy is associated with

$\hat{S} = -1$. In analogous magnetic language the tetragonal phase is then "paramagnetic" corresponding to $\langle \hat{S} \rangle = 0$ while the orthorhombic phase is "antiferromagnetic" with a nonzero *"staggered magnetization"*. In paramagnetic phase oxygen and vacancies are completely disordered and in the antiferromagnetic phase alternate ordering. The ordered arrangement of filled and vacant sites in the basal plane is predicted to be that shown in Fig.2.2a for planer concentration of oxygen c_o=0.5 ($\delta = 0$) and that shown in Fig.2.2b for $c_o = 0.25$ ($\delta = 0.5$) but both structures have orthogonal symmetry and will be denoted by OrthoI (at $\delta = 0$) and OrthoII ($\delta = 0.5$).

2.2 Spring-Defect Model

The science of physics assumes that physical phenomena may be explained and understood because of the functioning of physically real systems structured in certain ways and constituted of elements possessing certain properties. The exact nature of the real system in itself is usually unknown, so to gain an understanding of it a model (whose exact nature is known) is constructed. It is usually simple with all essential ingredients incorporated.

The model incorporates analogues of those aspects of the real system, which are relevant to the phenomena to be explained. We are just believing that the model gives us knowledge of the constitution of the real system. We are justified in believing that the model gives us knowledge of the constitution of the real system. Now we are going to Model the Cu-O basal plane of $YBa_2Cu_3O_{7-\delta}$ as a 2D-Ising system in which the copper atoms are assumed to be connected by spring constants 'K' along

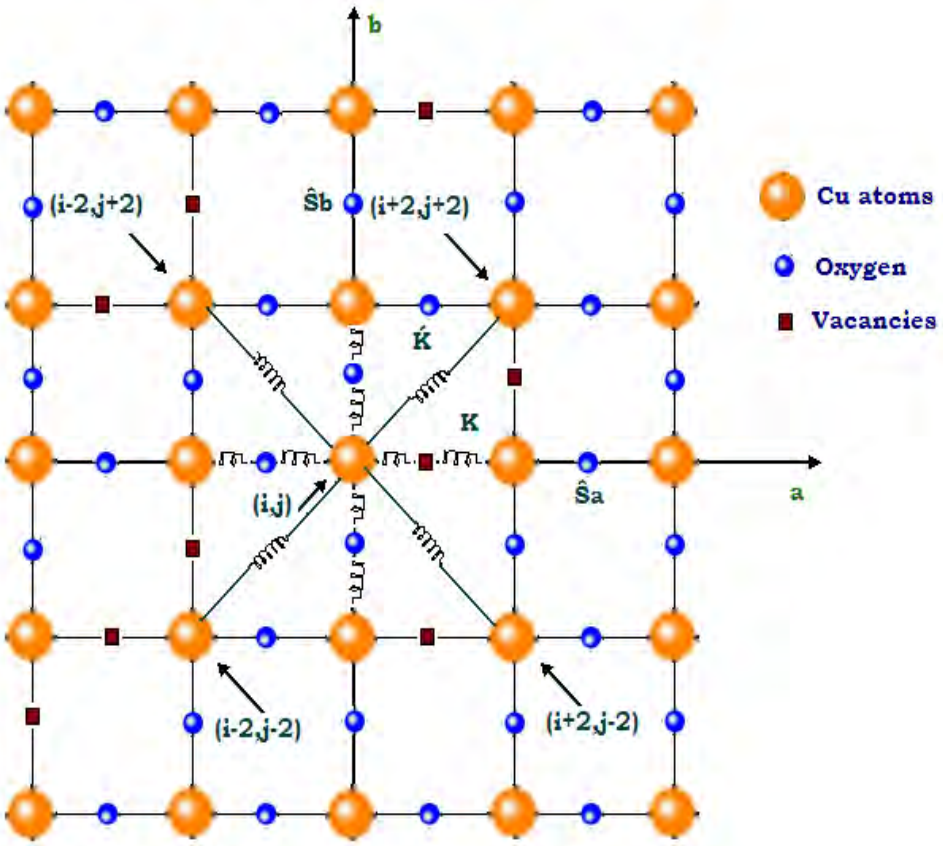

Figure 2.3: *Cu-O basal plane modeled as a 2D-Ising system with spring constants K and $K^{'}$, lattice constant a_0 and distortion parameter α. The pseudo-spin variables $\hat{S}_a$ and $\hat{S}_b$ have values ± 1 with a and b as sublattice indices.*

the chain and 'K'' along the diagonal (see Fig.2.3). The indices 'i' and 'j' run over all the lattice sites including the interstitial sites on which the oxygen resides. Now the potential energy in harmonic approximation is written as

$$\begin{aligned} V &= \sum_{i,j}\Bigg[\frac{1}{2}K'\Bigg[\Big\{([x(i+2,j+2)-x(i,j)]^2+[y(i+2,j+2)-y(i,j)]^2)^{\frac{1}{2}}-\sqrt{2a_0}\Big\}^2 \\ &+ \Big\{([x(i-2,j+2)-x(i,j)]^2+[y(i-2,j+2)-y(i,j)]^2)^{\frac{1}{2}}-\sqrt{2a_0}\Big\}^2 \\ &+ \Big\{([x(i+2,j-2)-x(i,j)]^2+[y(i+2,j-2)-y(i,j)]^2)^{\frac{1}{2}}-\sqrt{2a_0}\Big\}^2 \\ &+ \Big\{([x(i-2,j-2)-x(i,j)]^2+[y(i-2,j-2)-y(i,j)]^2)^{\frac{1}{2}}-\sqrt{2a_0}\Big\}^2\Bigg] \qquad (2.2.1) \\ &+ \frac{1}{2}K\Bigg[[x(i+2;j)-x(i;j)-a_0-\alpha\hat{S}_a(i+2,j)]^2+[y(i;j+2)-y(i;j)-a_0-\alpha\hat{S}_b(i,j+2)]^2 \\ &+ [x(i-2;j)-x(i;j)-a_0-\alpha\hat{S}_a(i-2,j)]^2+[y(i;j-2)-y(i;j)-a_0-\alpha\hat{S}_b(i,j-2)]^2\Bigg]\Bigg] \end{aligned}$$

where a_0 is the lattice constant for the un defected lattice and the parameter α is a measure of the distortion the lattice undergoes as a result of structural ordering. Let us now modify the value of x and y because of presence or absence of an oxygen atom by

$$x(i;j)=\bar{x}(i;j)+\xi(i;j);\ y(i;j)=\bar{y}(i;j)+\eta(i;j) \qquad (2.2.2)$$

where overbar are average equilibrium value and ξ and η are small fluctuation around

the mean values.

$$\begin{aligned}
\xi(i,j) &= \sum_{q_x,q_y} \xi(q_x,q_y)\exp\big[-\frac{ia_0}{2}(iq_x+jq_y)\big] \\
\eta(i,j) &= \sum_{q_x,q_y} \eta(q_x,q_y)\exp\big[-\frac{ia_0}{2}(iq_x+jq_y)\big] \\
\bar{x}(i,j) &= \frac{1}{2}a_0 i \\
\bar{y}(i,j) &= \frac{1}{2}a_0 j \\
\hat{S}_a(i,j) &= \sum_{q_x,q_y} \hat{S}_a(q_x,q_y)\exp\big[-\frac{ia_0}{2}(iq_x+jq_x)\big]
\end{aligned} \tag{2.2.3}$$

then we get

$$V(q)=\sum_q \Big\{A_q\left|\xi_q\right|^2+B_q\left|\eta_q\right|^2+C_q\{\xi_q\eta_q^*+\xi_q^*\eta_q\}-2\{G_q\hat{S}_q^a\xi_q^*+F_q\hat{S}_q^b\eta_q^*\}\Big\} \tag{2.2.4}$$

where

$$\begin{aligned}
A_q &= (K+K^{'})-\cos(a_0q_x)\big[K+K^{'}\cos(a_0q_y)\big] \\
B_q &= (K+K^{'})-\cos(a_0q_y)\big[K+K^{'}\cos(a_0q_x)\big] \\
C_q &= K^{'}\sin(a_0q_x)\sin(a_0q_y) \\
F_q &= iK\alpha\sin\big(\frac{a_0q_y}{2}\big) \\
G_q &= iK\alpha\sin\big(\frac{a_0q_x}{2}\big)
\end{aligned} \tag{2.2.5}$$

Let us now introduce the column vectors

$$U_q=\begin{bmatrix}\xi_q\\ \eta_q\end{bmatrix},\hat{S}_q=\begin{bmatrix}\hat{S}_q^a\\ \hat{S}_q^b\end{bmatrix},\chi_q=\begin{bmatrix}A_q & C_q\\ C_q & B_q\end{bmatrix},\psi_q=\begin{bmatrix}G_q & 0\\ 0 & F_q\end{bmatrix} \tag{2.2.6}$$

where ψ_q is the matrix of spin-strain coupling, U_q is the column vector of the displacements of all the atoms from their lattice sites, $\hat{S}_q$ is the column vector of all $\hat{S}_q^{a,b}$ and χ_q is the dynamical force matrix.

From equation (2.2.6) we obtain

$$\begin{aligned} U_q^\dagger &= \begin{bmatrix} \xi_q^* & \eta_q^* \end{bmatrix}, \hat{S}_q^\dagger = \begin{bmatrix} \hat{S}_q^a & \hat{S}_q^b \end{bmatrix}, \chi_q^\dagger = \begin{bmatrix} A_q^* & C_q^* \\ C_q^* & B_{q^*} \end{bmatrix} = \chi_q \\ \psi_q^\dagger &= \begin{bmatrix} G_q^* & 0 \\ 0 & F_q^* \end{bmatrix} = \psi_q \\ and\, \chi_q^{-1} &= \begin{bmatrix} -\frac{B_q}{C_q^2 - A_q B_q} & \frac{C_q}{C_q^2 - A_q B_q} \\ \frac{C_q}{C_q^2 - A_q B_q} & -\frac{A_q}{C_q^2 - A_q B_q} \end{bmatrix} \end{aligned} \tag{2.2.7}$$

Now let us modify equation (2.2.4) using the above matrices i.e.

$$A_q \left|\xi_q\right|^2 + B_q \left|\eta_q\right|^2 + C_q \left\{\xi_q \eta_q^* + \xi_q^* \eta_q\right\} = \bar{U}_q^\dagger \chi_q \bar{U}_q \tag{2.2.8}$$

and

$$2\left\{G_q \hat{S}_q^a \xi_q^* + F_q \hat{S}_q^b \eta_q^*\right\} = \hat{S}_q^\dagger \psi_q^\dagger \bar{U}_q + \bar{U}_q^\dagger \psi_q \hat{S}_q \tag{2.2.9}$$

by substituting equations (2.2.8) and (2.2.9) in equation (2.2.4) we get

$$V(q) = \sum_q \left\{\bar{U}_q^\dagger \chi_q \bar{U}_q - \hat{S}_q^\dagger \psi_q^\dagger \bar{U}_q - \bar{U}_q^\dagger \psi_q \hat{S}_q\right\} \tag{2.2.10}$$

the Hamiltonian can be decoupled by considering

$$\bar{U}_q = U_q - \chi_q^\dagger \psi_q \hat{S}_q \tag{2.2.11}$$

as a set of displaced "oscillator" coordinates. Using equation (2.2.11) we can transform equation (2.2.10) and we get

$$V(q) = \sum_q \left\{\bar{U}_q^\dagger \chi_q \bar{U}_q - \hat{S}_q^\dagger \psi_q^\dagger \chi_q^{-1} \psi_q \hat{S}_q\right\} \tag{2.2.12}$$

$$\hat{S}_q^\dagger \psi_q^\dagger \chi_q^{-1} \psi_q \hat{S}_q = \frac{1}{A_q B_q - C_q^2} \Big\{ B_q |G_q|^2 |\hat{S}_q^a|^2 \;-\; C_q G_q^* F_q \hat{S}_q^{*a} \hat{S}_q^b \;-\; C_q F_q^* G_q \hat{S}_q^a \hat{S}_q^{*b} + A_q |F_q|^2 |\hat{S}_q^b|^2 \Big\} \tag{2.2.13}$$

let us now introduce the effective interactions $J_{\mu\nu}(q)$ as

$$\begin{aligned} J_{aa}(q) &= \frac{B_q |G_q|^2|}{A_q B_q - C_q^2} \;,\; J_{bb}(q) = \frac{A_q |F_q|^2}{A_q B_q - C_q^2} \\ J_{ab}(q) &= -\frac{C_q G_q^* F_q}{A_q B_q - C_q^2} \;,\; J_{ba}(q) = -\frac{C_q F_q^* G_q}{A_q B_q - C_q^2} \end{aligned} \tag{2.2.14}$$

by substituting equations (2.2.13) and (2.2.14) in equation (2.2.12) we get

$$V(q) = \text{harmonic solid} + \text{defect-defect interaction}$$

$$V(q) = \sum_q \bar{U}_q^\dagger \chi_q \bar{U}_q - \sum_q \sum_{\mu\nu} J_{\mu\nu}(q) \hat{S}_\mu^*(q) \hat{S}_\nu(q) \tag{2.2.15}$$

where μ and ν are sublattice indices 'a ' and 'b'. The first term of equation (2.2.15) describes a harmonic solid and the second term is the defect-defect interaction. Only the second term contains the ordering variables ($\hat{S}_q$) coupled to one another by strain mediated interaction $J_{\mu\nu}$. As far as the static properties of the transformed Hamiltonian are concerned we can therefore ignore the lattice dynamics and phonon properties involving ($\bar{U}_q$) and focus entirely on the ordering variable ($\hat{S}_q$). In real space the defect-defect coupling can be rewritten as

$$H_{d-d} = -\sum_{r,r'} \sum_{\mu\nu=a,b} J_{\mu\nu}(r - r') \hat{S}_\mu(r) \hat{S}_\nu(r') \tag{2.2.16}$$

where $J_{\mu\nu}(r)$ is obtained by fourier-inversion of $J_{\mu\nu}(q)$. The basic message of equation (2.2.16) is that occurs an effective defect-defect interaction (even if the defects are far apart in the lattice) mediated by the host spring forces [15].

2.3 Static Effects

2.3.1 Strain-Strain Interaction

In the previous section we have discussed the model derived by Ghoshal and Gebayh [15] for the structural transition from tetragonal phase to the orthorhombic phase in $YBa_2Cu_3O_{7-\delta}$ [16] using the help of spring-defect model and we find the defect-defect Hamiltonian. The study of mechanical behavior of YBCO is very important for the fundamental applications in device. In technology, it would tell us about the strength of the materials. In fundamental research, it is of interest because of the inside it provides into the nature of the binding forces in solids.With the preceding background, we will explore in this chapter the natural connection between the presence of defects and the concomitant strain development in YBCO [17]. To do this we need to transform the Hamiltonian from spin variable to strain variables.

An oxygen interstitial defect creates an elastic (Zener) dipole with its long axis oriented either along the a or the b axis in the Cu-O plane. The Ising interaction between defects can then be recast in the equivalent form of a strain-strain interaction which describes a transition from a ferroelastic (orthorhombic) to a paraelastic (tetragonal) phase. Hence, all the phase transformation properties associated with the ferroelastic to paraelastic transition, e.g., the transition temperature T_c , the temperature variation of the order parameter, the compliance tenser, etc., can be analyzed in terms of the statistical mechanics of the underlying Ising model [18]. The important and original feature of our treatment is that every term of the strain-strain interaction, including the strain dipole tensor, is calculable from the parameters of the basic

spring-defect model. Thus, the treatment allows a connection to be established between not just ferroelasticity with defect-mediated structural transition but also with phonon properties of the host crystal.

In this subsection we will express the Hamiltonian for the spring-defect model as a strain-strain interaction.

In previous subsection, we explained that there occurs an effective defect-defect interaction if the oxygen is viewed as a defect causing local stretching of the host copper atoms, which are themselves coupled by harmonic springs in the Cu-O basal plane. In real space the defect-defect coupling was rewritten as

$$H_{d-d} = -\sum_{r,r'} \sum_{\mu\nu=a,b} J_{\mu\nu}(r-r')\hat{S}_{\mu}(r)\hat{S}_{\nu}(r') \tag{2.3.1}$$

Here we intend to rewrite and further analyze the Hamiltonian equation (2.3.1) in terms of the components which defines the deformation $\hat{\varepsilon}_{xx}$ and $\hat{\varepsilon}_{yy}$ of a spontaneous strain tensor operator associated with a and b sublattices, caused by the oxygen defects. A hat on the top of ε indicates the operator nature of the strain tensor. The z-component is not included here as it is not relevant for discussion of oxygen ordering, which is restricted to the Cu-O basal plane.

The strain field around each defect can be treated as an elastic dipole called zener dipole which is a strain ellipsoid whose major axis specifies the direction of anisotropy [19]. Such dipoles can be represented by a polar second rank tensor. In the spring-defect model, $\bar{U}_q$ is the displaced variable of a harmonic solid; as we know each atom makes simple harmonic vibration around its mean position so, its mean displacement

i.e., $\langle \bar{U}_q \rangle$ from its equilibrium position is zero therefore from equation (2.2.11) we have

$$\langle \bar{U}_q \rangle = \langle U_q - \chi_q^{-1} \psi_q \hat{S}_q \rangle = \langle U_q \rangle - \langle \chi_q^{-1} \psi_q \hat{S}_q \rangle = 0 \tag{2.3.2}$$

Let us consider some particular point in the sample whose position vector is $'r'$ (with components r_x, r_y) in the rectangular coordinate system in which the lattice is defined. The displacement vector at the position $'r'$ after the deformation takes place is denoted by $u(r)$ so that the deformation of the body is entirely determined by the two dimensional vectors u and r. Implicit in this description is the recognition that elasticity theory deals with the continuum [20]. Accordingly, the counterparts to the relations in equation (2.2.2) which were earlier written with the discrete nature of the lattice in mind, can be reexpressed as

$$\begin{aligned}
\big[u(r_x, r_y)\big]_x &= x(r_x, r_y) = \bar{x}(r_x, r_y) + \xi(r_x, r_y), \\
\big[u(r_x, r_y)\big]_y &= y(r_x, r_y) = \bar{y}(r_x, r_y) + \eta(r_x, r_y), \\
\xi(i,j) &= \int\int dq_x dq_y \xi(q_x, q_y) \exp\big\{ -i(r_x q_x + r_y q_y) \big\}, \\
\eta(i,j) &= \int\int dq_x dq_y \eta(q_x, q_y) \exp\big\{ -i(r_x q_x + r_y q_y) \big\},
\end{aligned} \tag{2.3.3}$$

using equation (2.2.6)

$$\chi_q^{-1} \psi_q \hat{S}_q = \begin{bmatrix} \hat{S}_q^b C_q \frac{F_q}{C_q^2 - A_q B_q} - \hat{S}_q^a B_q \frac{G_q}{C_q^2 - A_q B_q} \\ \hat{S}_q^a C_q \frac{G_q}{C_q^2 - A_q B_q} - \hat{S}_q^b A_q \frac{F_q}{C_q^2 - A_q B_q} \end{bmatrix}, \tag{2.3.4}$$

$$\begin{bmatrix} \langle \xi_q \rangle \\ \langle \eta_q \rangle \end{bmatrix} = \frac{1}{(C_q^2 + A_q B_q)} \begin{bmatrix} \langle \hat{S}_q^b \rangle C_q F_q - \langle \hat{S}_q^a \rangle B_q G_q \\ \langle \hat{S}_q^a \rangle C_q G_q - \langle \hat{S}_q^b \rangle A_q F_q \end{bmatrix}. \tag{2.3.5}$$

For small deformations the strain tensor is given by the usual expression of linear elasticity theory as

$$\varepsilon_{\alpha\beta}(r_x, r_y) = \frac{1}{2} \left(\frac{\partial u_\alpha(r)}{\partial r_\beta} + \frac{\partial u_\beta(r)}{\partial r_\alpha} \right), \tag{2.3.6}$$

in which α, β can take the values x and y. In the present we are considering only the components $\alpha = \beta =$ x or y as the oxygen defect has tetragonal symmetry. We know that a measure of the extent to which a body is deformed when it is subjected to a stress. The linear or tensile strain is the ratio of the change in length to the original length. Therefore, the relative elongations of the elements of length along the principle axes of the strain tensor (at a given point r) can be represented as

$$\varepsilon_{xx}(r_x, r_y) = \frac{\partial u_x(r)}{\partial r_x} = \frac{\xi(r_x, r_y)}{\frac{a_0}{2}} \tag{2.3.7}$$

similarly,

$$\varepsilon_{yy}(r_x, r_y) = \frac{\partial u_y(r)}{\partial r_y} = \frac{\eta(r_x, r_y)}{\frac{a_0}{2}} \tag{2.3.8}$$

and

$$\varepsilon_{xx}(q_x, q_y) = \frac{\xi(q_x, q_y)}{\frac{a_0}{2}} \ , \ \varepsilon_{yy}(q_x, q_y) = \frac{\eta(q_x, q_y)}{\frac{a_0}{2}}. \tag{2.3.9}$$

We may identify the x and y components of the strain tensor operator as

$$\hat{\varepsilon}_{xx}(q) = \frac{2}{a_0(A_q B_q - C_q^2)} \Big[B_q G_q \hat{S}_q^a - C_q F_q \hat{S}_q^b \Big] \tag{2.3.10}$$

and

$$\hat{\varepsilon}_{yy}(q) = \frac{2}{a_0(A_q B_q - C_q^2)} \Big[-C_q G_q \hat{S}_q^a + A_q F_q \hat{S}_q^b \Big] \tag{2.3.11}$$

In the usual treatments of anelasticity the strain dipole tensor is parameterized in terms of the so called λ-tensor [19]. By contrast, equations (2.3.10) and (2.3.11) provide explicitly calculated expressions in terms of the defect variables $\hat{S}_a$ and $\hat{S}_b$ and the parameters of the spring-defect model.

The converse relations by means of which we may map the spin variables $\hat{S}_a$ and $\hat{S}_b$ into the strain components i.e., when we rearrange the above equations (2.3.10) and

(2.3.11) we get

$$\hat{S}_a(q) = \frac{a_0}{2G_q}\Big[\hat{\varepsilon}_{xx}(q)A_q + \hat{\varepsilon}_{yy}(q)C_q\Big] \tag{2.3.12}$$

and

$$\hat{S}_b(q) = \frac{a_0}{2F_q}\Big[\hat{\varepsilon}_{xx}(q)C_q + \hat{\varepsilon}_{yy}(q)B_q\Big]. \tag{2.3.13}$$

Substituting in equation (2.2.15) i.e.,

$$\begin{aligned}\sum_{\mu\nu=a,b} J_{\mu\nu}(q)\hat{S}^*_\mu(q)\hat{S}_\nu(q) = \Big\{ & J_{aa}(q)\left|\hat{S}_a(q)\right|^2 \;+\; J_{ab}(q)\hat{S}^*_a(q)\hat{S}_b(q) \\ & +\; J_{ba}(q)\hat{S}^*_b(q)\hat{S}_a(q) + J_{bb}(q)\left|\hat{S}_b(q)\right|^2\Big\}\end{aligned} \tag{2.3.14}$$

now substituting the values J_{aa} , J_{ab} , J_{ba} *and* J_{bb} from equation (2.2.14) and for $\hat{S}_a$ *and* $\hat{S}_b$ from equation (2.3.12, 2.3.13) we get

$$\begin{aligned}\sum_{\mu\nu=a,b} J_{\mu\nu}(q)\hat{S}^*_\mu(q)\hat{S}_\nu(q) &= \frac{a_0^2}{4(A_qB_q - C_q^2)} \\ \times\Bigg[& - B_q\Big\{A_q^2\left|\hat{\varepsilon}_{xx}(q)\right|^2 + A_qC_q\hat{\varepsilon}^*_{xx}(q)\hat{\varepsilon}_{yy}(q) + A_qC_q\hat{\varepsilon}^*_{yy}(q)\hat{\varepsilon}_{xx}(q) + C_q^2\left|\hat{\varepsilon}_{yy}(q)\right|^2\Big\} \\ & - A_q\Big\{C_q^2\left|\hat{\varepsilon}_{xx}(q)\right|^2 + B_qC_q\hat{\varepsilon}^*_{xx}(q)\hat{\varepsilon}_{yy}(q) + B_qC_q\hat{\varepsilon}^*_{yy}(q)\hat{\varepsilon}_{xx}(q) + B_q^2\left|\hat{\varepsilon}_{yy}(q)\right|^2\Big\} \\ & + C_q\Big\{A_qC_q\left|\hat{\varepsilon}_{xx}(q)\right|^2 + A_qB_q\hat{\varepsilon}^*_{xx}(q)\hat{\varepsilon}_{yy}(q) + C_q^2\hat{\varepsilon}^*_{yy}(q)\hat{\varepsilon}_{xx}(q) + B_qC_q\left|\hat{\varepsilon}_{yy}\right|^2(q)\Big\} \\ & + C_q\Big\{A_qC_q\left|\hat{\varepsilon}_{xx}(q)\right|^2 + C_q^2\hat{\varepsilon}^*_{xx}(q)\hat{\varepsilon}_{yy}(q) + A_qB_q\hat{\varepsilon}^*_{yy}(q)\hat{\varepsilon}_{xx}(q) + B_qC_q\left|\hat{\varepsilon}_{yy}\right|^2(q)\Big\}\Bigg].\end{aligned} \tag{2.3.15}$$

Simplifying the above expression we get

$$\begin{aligned}\sum_{\mu\nu=a,b} J_{\mu\nu}(q)\hat{S}^*_\mu(q)\hat{S}_\nu(q) &= \frac{a_0^2}{4(A_qB_q - C_q^2)} \\ &\times\Bigg[- A_q(A_qB_q - C_q^2)\left|\hat{\varepsilon}_{xx}(q)\right|^2 - B_q(A_qB_q - C_q^2)\left|\hat{\varepsilon}_{yy}(q)\right|^2 \\ & - C_q(A_qB_q - C_q^2)\hat{\varepsilon}^*_{xx}(q)\hat{\varepsilon}_{yy}(q) - C_q(A_qB_q - C_q^2)\hat{\varepsilon}^*_{yy}(q)\hat{\varepsilon}_{xx}(q)\Bigg]\end{aligned} \tag{2.3.16}$$

then

$$\sum_{\mu\nu=a,b} J_{\mu\nu}(q)\hat{S}^*_\mu(q)\hat{S}_\nu(q) = \frac{a_{0^2}}{4}\Big[-A_q\,|\hat{\varepsilon}_{xx}(q)|^2 - B_q\,|\hat{\varepsilon}_{yy}(q)|^2 - C_q\hat{\varepsilon}^*_{xx}(q)\hat{\varepsilon}_{yy}(q) - C_q\hat{\varepsilon}^*_{yy}(q)\hat{\varepsilon}_{xx}(q)\Big] \tag{2.3.17}$$

now substituting this in equation (2.2.15) we get

$$\begin{aligned} V(q) &= \sum_q \bar{U}^\dagger_q \chi_q \bar{U}_q \qquad (2.3.18)\\ &- \sum_q \frac{a_{0^2}}{4}\Big[-A_q\,|\hat{\varepsilon}_{xx}(q)|^2 - B_q\,|\hat{\varepsilon}_{yy}(q)|^2 - C_q\hat{\varepsilon}^*_{xx}(q)\hat{\varepsilon}_{yy}(q) - C_q\hat{\varepsilon}^*_{yy}(q)\hat{\varepsilon}_{xx}(q)\Big] \end{aligned}$$

now we can rewrite the above equation (2.3.18) as

$$V(q) = \sum_q \bar{U}^\dagger_q \chi_q \bar{U}_q - \sum_q \sum_{\alpha,\beta=x,y} F_{\alpha\beta}(q)\hat{\varepsilon}^*_{\alpha\alpha}(q)\hat{\varepsilon}_{\beta\beta}(q) \tag{2.3.19}$$

where $F_{\alpha\beta}$ is the strength of the strain-strain coupling. Here α, β are the indices specifying the cartesian components and

$$F_{xx}(q) = -\frac{a_0^2}{4}A_q, \quad F_{yy}(q) = -\frac{a_0^2}{4}B_q, \quad F_{xy}(q) = F_{yx}(q) = -\frac{a_0^2}{4}C_q \tag{2.3.20}$$

in real space the strain-strain coupling can therefore be rewritten as

$$H_{s-s} = -\sum_{r,r'} \sum_{\alpha,\beta=x,y} F_{\alpha\beta}(r-r')\hat{\varepsilon}_{\alpha\alpha}(r)\hat{\varepsilon}_{\beta\beta}(r') \tag{2.3.21}$$

where $F_{\alpha\beta}(r)$ is obtained by Fourier-inversion of $F_{\alpha\beta}(q)$. This analysis then provides an interesting connection between the spring-defect model, which has been proposed from basic lattice dynamical considerations, and a model of strain-strain coupling, which is immediately applicable to the study of phenomena such as anelasticity, ferroelasticity, etc.

2.3.2 Mean Field Treatment of The Hamiltonian

The numerical results for the strain induced coupling (J_{ij}) between Ising spins show that the long range interaction between oxygen defects mediated by the host lattice makes an important contribution towards the order-disorder phase transition in YBCO [16]. The detailed Statistical mechanical analysis of the Hamiltonian given in Equation (2.3.1) is very complicated. Here, however, our aim is to understand its properties qualitatively and their influence on the ferroelastic response, hence we use the mean-field approximation (MFA) [21, 22].

In field theory, the Hamiltonian may be expanded in terms of the magnitude of fluctuations around the mean of the field. In this context, MFT can be viewed as the "zeroth-order" expansion of the Hamiltonian in fluctuations. Physically, this means a MFT system has no fluctuations, but this coincides with the idea that one is replacing all interactions with a "mean field".

Now we are going to find the order parameter with the help of mean field approximation (MFA). The defect-defect Hamiltonian in the absence of external field is given by

$$H_{d-d} = -\sum_{r,r'}\sum_{\mu\nu=a,b} J_{\mu\nu}(r-r')\hat{S}_{\mu}(r)\hat{S}_{\nu}(r') \tag{2.3.22}$$

where $\hat{S}_{\mu}(r)$ and $\hat{S}_{\nu}(r')$ is a vector at the r^{th} and r'^{th} site respectively with $\left|\hat{S}_{\mu}(r)\right| = \left|\hat{S}_{\nu}(r')\right| = \pm 1$ and r, r' means the nearest neighbor and the next nearest neighbor pairs i.e., it labels the links on the lattice. Then taking the mean of equation (2.3.22) we get

$$\langle H_{d-d}\rangle = -\sum_{r,r'}\sum_{\mu\nu=a,b} J_{\mu\nu}(r-r')\langle\hat{S}_{\mu}(r)\hat{S}_{\nu}(r')\rangle \tag{2.3.23}$$

and from

$$\Delta X = \left\langle X^2 \right\rangle - \left\langle X \right\rangle^2 = 0$$

because MFT can be viewed as "Zeroth order" fluctuation. This consists of decoupling the correlation function as in the following:

$$\langle\, \hat{S}_\mu(r)\hat{S}_\nu(r')\,\rangle = \langle\, \hat{S}_\mu(r)\,\rangle\langle\, \hat{S}_\nu(r')\,\rangle = m_\mu(r)m_\nu(r') \tag{2.3.24}$$

So the mean-field Hamiltonian is

$$H_{MFA} = -\sum_{r,r'}\sum_{\mu\nu=a,b} J_{\mu\nu}(r-r')\langle\, \hat{S}_\mu(r)\hat{S}_\nu(r')\,\rangle \tag{2.3.25}$$

$$H_{MFA} = -\sum_{r}\sum_{r'}\sum_{\nu}\sum_{\mu} J_{\mu\nu}(r-r')\langle\, \hat{S}_\mu(r)\,\rangle\langle\, \hat{S}_\nu(r')\,\rangle \tag{2.3.26}$$

$$H_{MFA} = -\sum_{r}\sum_{r'}\sum_{\nu}\left\{ J_{a\nu}(r-r')\hat{S}_a(r)\langle\, \hat{S}_\nu(r')\,\rangle + J_{b\nu}(r-r')\hat{S}_b(r)\langle\, \hat{S}_\nu(r')\,\rangle \right\}. \tag{2.3.27}$$

Hence the effective Hamiltonian in the MFA has the form of

$$H_{MFA} = -\sum_{r}\hat{S}_a(r)f_a(r) - \sum_{r}\hat{S}_b(r)f_b(r) \tag{2.3.28}$$

where

$$f_a(r) = \sum_{r'}\sum_{\nu=a,b} J_{a\nu}(r-r')m_\nu(r') \tag{2.3.29}$$

and

$$f_b(r) = \sum_{r'}\sum_{\nu=a,b} J_{b\nu}(r-r')m_\nu(r'). \tag{2.3.30}$$

Equation (2.3.28) describes the Hamiltonian for the system in which the interaction due to the other defects is represented by an effective internal field $f_a(r)$ acting on the defect on the sublattice 'a' and $f_b(r)$ acting on the defect on the sublattice 'b'.

Hence one expects the mean values can be computed with negligible error by using the canonical distribution; i.e., one can write

$$m_a(r) = \langle \hat{S}_a(r) \rangle = \frac{Tr\Big[\hat{S}_a(r) \exp\{-\beta\, H_{MFA}\}\Big]}{Z}. \tag{2.3.31}$$

The partition function 'Z' is defined as 'sum over all states' i.e., $\hat{S}_a(r) = \hat{S}_b(r) = \pm 1$ or the *partition function* is given by

$$Z = Tr\Big[\exp\{-\beta H_{MFA}\}\Big] \tag{2.3.32}$$

we know that all quantities of interest can be calculated from the partition function.

$$m_a(r) = \frac{\sum_{\hat{S}_a(r),\hat{S}_b(r)=\pm 1} \Big\{\exp[-\beta\, H_{MFA}] * \hat{S}_a(r)\Big\}}{\sum_{\hat{S}_a(r),\hat{S}_b(r)=\pm 1} \exp\{-\beta\, H_{MFA}\}} \tag{2.3.33}$$

$$m_a(r) = \frac{\sum_{\hat{S}_a(r),\hat{S}_b(r)} \hat{S}_a(r) \exp\Big\{\beta(\sum_r \hat{S}_a(r) f_a(r) + \sum_r \hat{S}_b(r) f_b(r))\Big\}}{\sum_{\hat{S}_a(r),\hat{S}b(r)} \exp\Big\{\beta(\sum_r \hat{S}_a(r) f_a(r) + \sum_r \hat{S}_b(r) f_b(r))\Big\}}. \tag{2.3.34}$$

By summing first over all possible values of $\hat{S}_a(r)$, using the multiplicative property of the exponential function, and rearranging the order of summation of equation (2.3.34) can be also be written in the form of

$$m_a(r) = \frac{\sum_{\hat{S}_a(r)=\pm 1} \hat{S}_a(r) \exp\Big\{\beta(\sum_r \hat{S}_a(r) f_a(r))\Big\} * \sum_{\hat{S}_b(r)=\pm 1} \exp\Big\{\beta(\sum_r \hat{S}_b(r) f_b(r))\Big\}}{\sum_{\hat{S}_a(r)=\pm 1} \exp\Big\{\beta(\sum_r \hat{S}_a(r) f_a(r))\Big\} * \sum_{\hat{S}_b(r)=\pm 1} \exp\Big\{\beta(\sum_r \hat{S}_b(r) f_b(r))\Big\}} \tag{2.3.35}$$

then the last term in denominator and numerator is equal can be simplified and replacing for the value of $\hat{S}_a(r) = \pm 1$ we get

$$m_a(r) = \frac{\exp\Big\{\beta(\sum_r f_a(r))\Big\} - \exp\Big\{-\beta(\sum_r f_a(r))\Big\}}{\exp\Big\{\beta(\sum_r f_a(r))\Big\} + \exp\Big\{-\beta\big(\sum_r f_a(r)\big)\Big\}} \tag{2.3.36}$$

$$m_a(r) = \tanh\Big\{\beta\big(\sum_r f_a(r)\big)\Big\} \tag{2.3.37}$$

$$m_a(r) = \tanh\Big\{\beta\big(\sum_{r,r'}\sum_{\nu=a,b} J_{a\nu}(r-r')m_\nu(r')\big)\Big\}. \tag{2.3.38}$$

Similarly

$$m_b(r) = \tanh\Big\{\beta\big(\sum_{r,r'}\sum_{\nu=a,b} J_{b\nu}(r-r')m_\nu(r')\big)\Big\}. \tag{2.3.39}$$

Let us now define the order parameter as

$$Q_q = \int\int \alpha Q(r_x, r_y) dr_x dr_y \tag{2.3.40}$$

$$Q(r_x, r_y) = \langle \hat{S}_a(r) - \hat{S}_b(r)\rangle \tag{2.3.41}$$

where

$$Q(r_x, r_y) = \int\int dq_x dq_y \exp\big[i\big(q_x r_x + q_y r_y\big)\big]\left\{\big\langle \hat{S}_a(q_x, q_y)\big\rangle - \exp\big[\frac{ia_0}{2}(q_x - q_y)\big]\big\langle \hat{S}_b(q_x, q_y)\big\rangle\right\}. \tag{2.3.42}$$

From equation (2.3.40) we get

$$Q_q = \int \alpha\big\langle \hat{S}_a(r) - \hat{S}_b(r)\big\rangle dr \tag{2.3.43}$$

where

$$\hat{S}_a(r) = \int\int dq_x dq_y \hat{S}_a(q_x, q_y)\exp\big[i(q_x r_x + q_y r_y)\big] \tag{2.3.44}$$

and

$$\hat{S}_b(r) = \int\int dq_x dq_y \hat{S}_b(q_x, q_y)\exp\left\{i\big[q_x(r_x + \frac{a_0}{2}) + q_y(r_y - \frac{a_0}{2})\big]\right\}. \tag{2.3.45}$$

Now we can rewrite equation (2.3.43) i.e., an order parameter Q_q with wave vector q=0 as

$$Q_0 = \alpha\int \big[m_a(r) - m_b(r)\big]dr = \alpha\big[m_a(q=0) - m_b(q=0)\big] \tag{2.3.46}$$

where Q_0 is the staggered magnetization. In order to find the T_s at which the phase

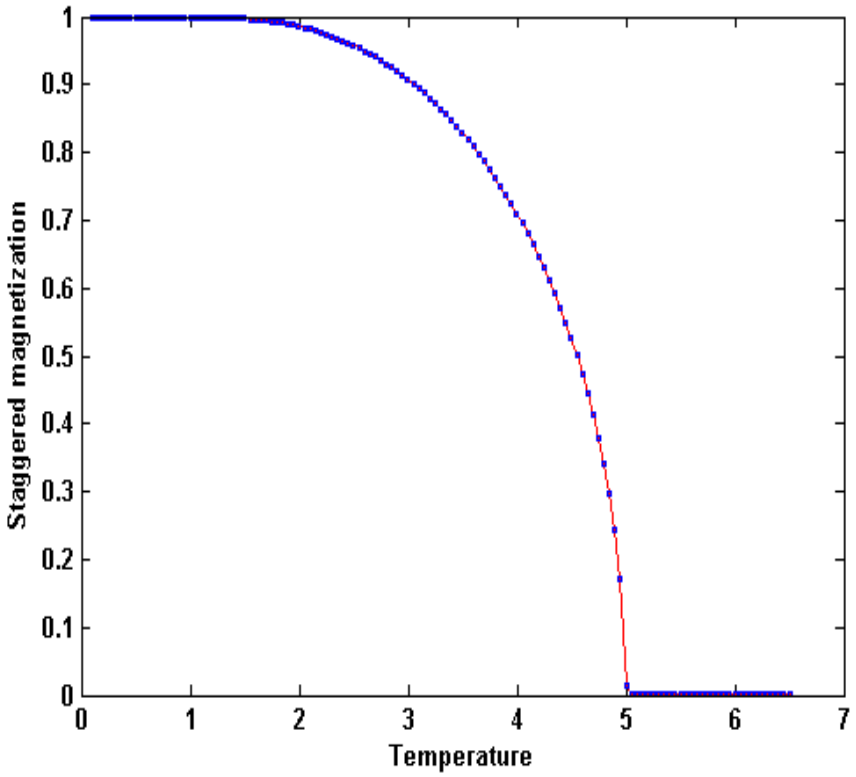

Figure 2.4: *Phase diagram of staggered magnetization vs. temperature. The transition temperature T_s is in the unit of $1/k_B$ where k_B is the Boltzman constant.*

transition takes place, we have to solve the transcendental equations (2.3.38) and (2.3.39) numerically. The resultant Q_0 vs T plot shows a second order phase curve also called *"continuous phase transitions"*, as shown in figure (2.4). The parameter Q_0 is indeed the order parameter for tetragonal to orthorhombic structural transition, as it is a measure of the spontaneous stretching of the lattice along a preferred axis. When the staggered magnetization $= 0$ one is in the disordered high-temperature phase while for staggered magnetization $\neq 0$, one is in the low-temperature ordered phase with net staggered magnetization. Alternatively, Q_0 can also be interpreted as

the ferroelastic order parameter by reexpressing $\hat{S}_a$ and $\hat{S}_b$ in terms of the strain tensor components, as in equations (2.3.12) and (2.3.13). Here finite 'Q' means oxygen-vacancy ordering (orthorhombic) and Q=0 mean complete disorder (tetragonal).

2.4 Static Compliance

In order to find the compliance or the susceptibility which yields the linear response to a stress, let us examine the expectation value of the strain in the system (having surface area Λ) when a small uniaxial stress σ is applied along the 'y' direction. The Hamiltonian now takes the form:

$$H = H_{MFA} + H_0 = H_{MFA} - \Lambda \sum_r \sigma_{yy}(r)\hat{\varepsilon}_{yy}(r). \tag{2.4.1}$$

Using equation (2.3.11) and

$$\hat{\varepsilon}_{yy}(r) = \sum_q \hat{\varepsilon}_{yy}(q) \exp\{-iq.r\}$$

we can rewrite H_0 as

$$H_0 = -\Lambda \sum_r \sigma_{yy}(r) \sum_q \hat{\varepsilon}_{yy}(q) \exp\{-iq.r\}. \tag{2.4.2}$$

$$H_0 = -\Lambda \sum_r \sigma_{yy}(r) \sum_q \left\{ \frac{2\exp\{-iq.r\}}{a_0(A_qB_q - C_q^2)} \left[-C_qG_q\hat{S}_a(q) + A_qF_q\hat{S}_b(q) \right] \right\} \tag{2.4.3}$$

$$H_0 = -\Lambda \sum_r \sum_{q'} \sigma_{yy}(q') \exp\{-iq'.r\} \sum_q \exp\{-iq.r\} \left\{ \frac{2}{a_0(A_qB_q - C_q^2)} \Big[-C_qG_q\hat{S}_a(q) + A_qF_q\hat{S}_b(q) \Big] \right\} \tag{2.4.4}$$

$$\begin{aligned} H_0 \;=\; & -\Lambda \sum_r \sum_{q'} \sigma_{yy}(q') \exp\{-iq'.r\} \sum_q \exp\{-iq.r\} \left\{ \frac{2}{a_0(A_qB_q - C_q^2)} \Big[-C_qG_q \right. \\ & \left. \sum_{r'} \hat{S}_a(r') \exp\{iq.r'\} + A_qF_q \sum_{r'} \hat{S}_b(r') \exp\{iq.r'\} \Big] \right\} \end{aligned} \tag{2.4.5}$$

$$H_0 = -\Lambda \sum_{q'} \sum_{q} \sum_{r} \sigma_{yy}(q') \exp\{-i(q'+q)r\} \Big\{ \frac{2}{a_0(A_q B_q - C_q^2)} \sum_{r'} \exp\{iq.r'\} \Big[-C_q G_q \hat{S}_a(r') + A_q F_q \hat{S}_b(r') \Big] \Big\}. \tag{2.4.6}$$

We can now change $r' \to r$, $q' \to q$ and $q \to -q$ because they are dummy variables

$$H_0 = -\Lambda \sum_{r} \sum_{q} \sigma_{yy}(q) \frac{2\exp\{-iq.r\}}{a_0(A_q B_q - C_q^2)} \Big[-C_q G_q^* \hat{S}_a(r) + A_q F_q^* \hat{S}_b(\mathbf{r}) \Big] \tag{2.4.7}$$

$$H_0 = \sum_{r} h_a(r) \hat{S}_a(r) + \sum_{r} h_b(r) \hat{S}_b(r) \tag{2.4.8}$$

where

$$h_a(r) = \frac{2\Lambda}{a_0} \sum_{q} \sigma_{yy}(q) \frac{C_q G_q^*}{(A_q B_q - C_q^2)} \exp\{-iq.r\} \tag{2.4.9}$$

and

$$h_b(r) = -\frac{2\Lambda}{a_0} \sum_{q} \sigma_{yy}(q) \frac{A_q F_q^*}{(A_q B_q - C_q^2)} \exp\{-iq.r\}. \tag{2.4.10}$$

Now we can rewrite H_0 as

$$H_0 = \sum_{r} \sum_{\mu=a,b} h_\mu(r) \hat{S}_\mu(r), \tag{2.4.11}$$

where $h_\mu(r)$ is a fictitious field which is expressible in terms of the applied stress and the other microscopic parameters of the model.

Now the order parameter equation in the presence of an external field can be written as

$$m_a(r) = \tanh\Big\{ \beta \Big(\sum_{r,r'} \Big(\sum_{\nu=a,b} J_{a\nu}(r-r')\, m_\nu(r') + h_a(r) \Big) \Big) \Big\} \tag{2.4.12}$$

similarly

$$m_b(r) = \tanh\Big\{ \beta \Big(\sum_{r,r'} \Big(\sum_{\nu=a,b} J_{b\nu}(r-r')\, m_\nu(r') + h_b(r) \Big) \Big) \Big\}. \tag{2.4.13}$$

Let now linearize both sides i.e.,

$$m_a(r) \simeq \beta\Big\{ \sum_{r,r'}\Big(\sum_{\nu=a,b} J_{b\nu}(r-r')\, m_\nu(r') + h_a(r)\Big)\Big\} \tag{2.4.14}$$

whose Fourier transform becomes

$$m_a(q) \simeq \beta\Big\{ \sum_{\nu=a,b} J_{a\nu}(q)\, m_\nu(q) + h_a(q)\Big\}. \tag{2.4.15}$$

Now the stress tensor in terms of the strain tensor can be written as

$$\sigma_{\mu\nu}(q) = L_{\mu\nu\alpha\beta}(q)\big\langle\, \hat{\varepsilon}_{\alpha\beta}(q)\,\big\rangle \tag{2.4.16}$$

where $L_{\mu\nu\alpha\beta}(q)$ is the "*elastic modulus tensor*". Here we adopted the usual convention of summation over repeated Greek indices. Since the applied stress is uniaxial and along the 'y' direction of the rectangular sample, $\mu = \nu = y$ and $\alpha = \beta = x$ or 'y' directions only. Denoting

$$L_{yyxx}(q) = \lambda^{(1)} \;\; and \;\; L_{yyyy}(q) = \lambda^{(2)}$$

we obtain then

$$\sigma_{yy}(q) = \lambda^{(1)}(q)\big\langle\, \hat{\varepsilon}_{xx}(q)\,\big\rangle + \lambda^{(2)}(q)\big\langle\, \hat{\varepsilon}_{yy}(q)\,\big\rangle. \tag{2.4.17}$$

The converse relation to equation (2.4.17) is the one in which the strain tensor is written in terms of the stress tensor as,

$$\hat{\varepsilon}_{\mu\nu}(q) = \Gamma_{\mu\nu\alpha\beta}(q)\big\langle\, \sigma_{\alpha\beta}(q)\,\big\rangle \tag{2.4.18}$$

where $\Gamma_{\mu\nu\alpha\beta}(q)$ is the "*compliance (susceptibility) tensor*" with $\hat{L}\hat{\Gamma} = 1$.

In order to obtain the expression for the modulus we first write $m_b(q)$ in terms of $m_a(q)$ i.e.,

$$m_a(q) \simeq \beta\big\{ J_{aa}(q)m_a(q) + J_{ab}(q)m_b(q) + h_a(q)\big\} \tag{2.4.19}$$

and

$$m_b(q) \simeq \beta\big\{J_{ba}(q)m_a(q) + J_{bb}(q)m_b(q) + h_b(q)\big\} \tag{2.4.20}$$

$$m_b(q) \simeq \frac{\beta J_{ba}(q)}{1-\beta J_{bb}(q)} m_a \; + \; \frac{\beta h_b(q)}{1-\beta J_{bb}(q)} \tag{2.4.21}$$

now substituting equation (2.4.21) in equation (2.4.19) we get

$$m_a(q) = \beta\Big[J_{aa}(q)m_a(q) + J_{ab}(q)\Big(\frac{\beta J_{ba}(q)}{1-\beta J_{bb}(q)} m_a \; + \; \frac{\beta h_b(q)}{1-\beta J_{bb}(q)}\Big) + h_a(q)\Big] \tag{2.4.22}$$

then we get

$$\begin{aligned} m_a(q)\Big[1 \;\; - \;\; & \beta\big\{J_{aa}(q) + J_{bb}(q)\big\} + \beta^2\big\{J_{aa}(q)J_{bb}(q) - J_{ab}(q)J_{ba}(q)\big\}\Big] \\ = \;\; & \beta^2\big\{J_{ab}(q)h_b(q) - J_{bb}(q)h_a(q)\big\} + \beta\, h_a(q). \end{aligned} \tag{2.4.23}$$

Let now substituting the values for $J_{aa}, J_{bb}, J_{ab}, J_{ba}$ from equation (2.2.14) and $m_a = \big\langle \hat{S}_a \big\rangle$ from equation (2.3.12) and

$$h_a(q) = \frac{2\Lambda C_q G_q^*}{a_0(A_qB_q - C_q^2)}\sigma_{yy} \; and \; h_b(q) = -\frac{2\Lambda A_q F_q^*}{a_0(A_qB_q - C_q^2)}\sigma_{yy}.$$

Then we get

$$\frac{2\Lambda\beta C_q G_q^*}{a_0}\sigma_{yy}(q) = m_a(q)\Big[\big(A_qB_q - C_q^2\big) - \beta\left(B_q\left|G_q\right|^2 + A_q\left|F_q\right|^2\right) + \beta^2\left(\left|G_q\right|^2\left|F_q\right|^2\right)\Big] \tag{2.4.24}$$

$$\begin{aligned} \sigma_{yy}(q) \;\; = \;\; & \big(\frac{a_0}{2G_q}\big)\big(\frac{a_0}{2\Lambda\beta C_q G_q^*}\big)\Big[\big\langle\hat{\varepsilon}_{xx}(q)\big\rangle A_q + \big\langle\hat{\varepsilon}_{yy}(q)\big\rangle C_q\Big] \\ \times \;\; & \Big[\big(A_qB_q - C_q^2\big) - \beta\left(B_q\left|G_q\right|^2 + A_q\left|F_q\right|^2\right) + \beta^2\left(\left|G_q\right|^2\left|F_q\right|^2\right)\Big]. \end{aligned} \tag{2.4.25}$$

We get finally the expression for $\sigma_{yy}(q)$ in terms of $\big\langle\hat{\varepsilon}_{xx}\big\rangle, \big\langle\hat{\varepsilon}_{yy}\big\rangle$ and all other basic microscopic parameters of the model. Comparing the expression of $\sigma_{yy}(q)$ with equation (2.4.17) we note that the elastic modulus for $\lambda^{(1)}(q)$ and $\lambda^{(2)}(q)$ becomes.

$$\lambda^{(1)}(q) = \frac{a_0^2 A_q\Big[(A_qB_q - C_q^2) - \beta(B_q\left|G_q\right|^2 + A_q\left|F_q\right|^2) + \beta^2(\left|G_q\right|^2\left|F_q\right|^2)\Big]}{4\Lambda\beta C_q\left|G_q\right|^2} \tag{2.4.26}$$

and

$$\lambda^{(2)}(q) = \frac{a_0^2\Big[(A_qB_q - C_q^2) - \beta(B_q\left|G_q\right|^2 + A_q\left|F_q\right|^2) + \beta^2(\left|G_q\right|^2\left|F_q\right|^2)\Big]}{4\Lambda\beta\left|G_q\right|^2} \tag{2.4.27}$$

inverting the expressions for $\lambda^{(1)}(q)$ and $\lambda^{(2)}(q)$ we get the corresponding expressions for the static compliance $\chi^{(1)}(q)$ and $\chi^{(2)}(q)$ respectively, where $\Gamma_{yyxx}(q) = \chi^{(1)}(q)$ and $\Gamma_{yyyy}(q) = \chi^{(2)}(q)$.Thus we have

$$\chi^{(2)}(q) = \frac{4\Lambda\beta\left|G_q\right|^2}{a_0^2\Big[(A_qB_q - C_q^2) - \beta(B_q\left|G_q\right|^2 + A_q\left|F_q\right|^2) + \beta^2(\left|G_q\right|^2\left|F_q\right|^2)\Big]}. \tag{2.4.28}$$

Similarly we can get the expression for $\chi^{(1)}(q)$ from equation (2.4.26) by inverting the expression for $\lambda^{(1)}(q)$. In the high temperature limit (highly disorder phase) the above expression reduces to the expected Curie form i.e.,

$$\chi^{(2)}(q) \simeq \frac{4\Lambda\beta\left|G_q\right|^2}{a_0^2\Big[(A_qB_q - C_q^2)\Big]}. \tag{2.4.29}$$

The expected Curie-Weiss-Ornstein-Zernike form of the static compliance which obtained when the transition temperature is approached from the disordered phase, is arrived at by neglecting terms of order β^2 from equation (2.4.28), thus

$$\begin{aligned}
\chi^{(2)}(q) &\simeq \frac{4\Lambda\beta\left|G_q\right|^2}{a_0^2\Big[(A_qB_q - C_q^2) - \beta(B_q\left|G_q\right|^2 + A_q\left|F_q\right|^2)\Big]} \\
&\simeq \frac{4\Lambda\left|G_q\right|^2}{a_0^2\Big[\frac{1}{\beta}(A_qB_q - C_q^2) - (B_q\left|G_q\right|^2 + A_q\left|F_q\right|^2)\Big]} \\
&\simeq \frac{4\Lambda\left|G_q\right|^2}{a_0^2k_B\big(A_qB_q - C_q^2\big)\Big(T - \frac{B_q|G_q|^2 + A_q|F_q|^2}{k_B(A_qB_q - C_q^2)}\Big)}.
\end{aligned} \tag{2.4.30}$$

We can rewrite this as

$$\chi^{(2)}(q) \simeq \frac{4\Lambda\left|G_q\right|^2 \Big/ a_0^2k_B(A_qB_q - C_q^2)}{\Big(T - \frac{B_q|G_q|^2 + A_q|F_q|^2}{k_B(A_qB_q - C_q^2)}\Big)} \tag{2.4.31}$$

the transition temperature T_s, defined as

$$T_s = \lim_{q \to 0} \frac{B_q \left|G_q\right|^2 + A_q \left|F_q\right|^2}{k_B\big(A_q B_q - C_q^2\big)} \tag{2.4.32}$$

is the frroelastic transition temperature at which the compliance (to an applied uniform stress) diverges. In real space the static compliance takes the form

$$\chi^{(j)}(r) = \sum_q \chi^{(j)}(q) \exp\{-iq.r\}\,,\ where\ j = 1\ or\ 2$$

The Curie-Weiss law for static compliance is as the system develops a spontaneous strain while undergoing a transition from the high temperature tetragonal phase to the low temperature orthorhombic phase. This approach is based on the premise that the structural transition and the concomitant ferroelasticity in YBCO are driven by loosely bound oxygen interstitial atoms in the CuO plane. Our method relies on a fully statistical mechanical treatment of a microscopic Hamiltonian. Further, our theory has unique transition temperature T_s which characterizes the tetragonal to orthorhombic transformation as well as the paraelastic to ferroelastic transition. This estimate of transition temperature is however very rough and qualitative. To get accurate estimate of the temperature one must deal with 3-dimensional model.

Chapter 3

Relaxational Effects

3.1 Introduction

In chapter two we addressed the issue of paraelastic to ferroelastic transition concomitant with tetragonal to orthorhombic structural phase transformation in the high T_c system YBCO. Orthorhombicity is associated with the formation of oxygen chains in the two-dimensional Cu-O basal plane as a consequence of ordering of oxygen atoms in preferential sublattice positions in 'b' sublattice direction. The theme of the spring-defect model treated in chapter 2 was further expanded to strain-strain interaction by associating with each oxygen atom a *"Zener-dipole"* [17]. This allowed us to give a microscopic basis of ferroelasticity in YBCO and in addition, study the compliance of the system, i.e., the response to an applied stress [27].

In this chapter we complement our treatment in chapter two by investigating the corresponding dynamical effects of the paraelastic to ferroelastic transition [28]. The

spring-defect model provides a natural setting for analyzing dynamics, as the hopping of oxygen atoms from occupied to vacant sites renders the Hamiltonian time-dependent. This time-dependence is stochastic in nature, caused by random exchanges of oxygen atoms and vacancies, as described by the so called Kawasaki process of the underlying Ising model [26]. In terms of the strain variables, each Kawasaki jump, assumed to occur amongst nearest neighbor sites, triggers a flip in the orientation of the principal axis of the strain tensor. This dynamics can be studied by subjecting the system to a small uniaxial stress, say along the b-axis. By relating the strain variables to oxygen occupation variables we investigate the time-evolution of the macroscopic strain tensor, and in particular, its linear response to the applied stress. The latter yields the response function, and via the response-relaxation relationship, the frequency-dependent compliance [29]. Like in chapter 2 our analysis is restricted to mean field theory, which is expected to provide a good approximation scheme in view of the long range nature of the strain interactions. Naturally therefore, the static form of the compliance derived in chapter 2 follows as a special case of our result, in the zero frequency limit.

Our work is motivated by a number of experimental investigations which have indicated the occurrence of stress induced diffusive hopping of oxygen atoms in YBCO see [25, 30]. Internal friction and resonant frequency measurements have been carried out in $YBa_2Cu_3O_{7-x}$; after oxygen outgassing the material becomes semiconducting $YBa_2Cu_3O_6$ and the anelastic processes observed in the superconducting samples are suppressed. Instead, a new intense effect appears, the process is thermally activated (shifting from 56 to 75 K when the frequency changes from 1.1 to 17.4 kHz) with an activation energy Es=0.11 eV, and is only 25% broader than a single relaxation

time process. It is attributed to the stress-induced hopping of residual free oxygen and the derived diffusion coefficient is D=410-4exp(-0.11 eV/kT) cm^2/sec, which extrapolated to room temperature is comparable with that of hydrogen in transition metals [31]. The issue of oxygen diffusion is important, not only in connection with carrier motion in the superconducting phase, but also in determining the switching of ferroelastic domains across walls an order-disorder phase transition in a crystal has been developed with strain-induced coupling between Ising spins. Strain coupling leads to long-ranged renormalized interactions between the spins which result in ferroelastic-antiferroelastic phase transitions [32]. Measurements of the elastic behavior of YBCO by internal friction and ultrasonic attenuation technique [33] shows a strong softening of the elastic constants at T=210K indicating, the development of a structural instability at this temperature. The experiment of Bonetti et al, 1991 [34] in polycrystalline YBCO using vibrating reed technique ($10^2 - 10^4 Hz$) shows an abrupt and strong modulus softening at the onset of structural phase transition and hence the emergence of ferroelasticity.

In the section 2 we are going to introduce the kinetic equations based on the Kawasaki model in the context of the spring-defect model, within mean field theory. From the mean field version of these equations we develop, in section 3 the main part of this chapter in which the anelastic relaxation as the system undergoes paraelastic to ferroelastic transition, is studied in detail. Finally our main results will be summarized.

3.2 Kinetics of Strain Model Using Mean Field Theory

We turn our attention now to the kinetics of the order-disorder transition. In the context of YBCO, kinetic processes are governed by microscopic jumps of the oxygen atoms into vacant sites induced by thermal fluctuations. The latter, while being always present even when the system is in thermal equilibrium, can lead to biased diffusion in the presence of ordering interactions. In the pseudo-spin language one imagines that the spin system described by equation (2.2.16) is in contact with a heat bath which causes spontaneous spin exchanges between two sites i and j at random instants of time. Thus, for example, a transition of the variable $\hat{S}_i$ from the value +1 to -1 is accompanied by a simultaneous transition of the variable $\hat{S}_j$ from the value -1 to +1 (site i and j are nearest neighbors). This process would obviously mimic the hopping of the impurity atom from site i to site j. The appropriate master equation for the time evolution of the probability of a certain spin configuration, which specifies completely the kinetics of the problem, was written down by Kawasaki [26].

We note that although the Kawasaki process conserves the number of oxygen atoms, the *"staggered magnetization"* which is the appropriate order parameter for the underlying *"antiferromagnetic"* ordering remains non conserved. A rigorous treatment of such a kinetic process is quite complicated. Here, however, we adopt a simpler picture in which the antiferromagnetically ordered lattice may be viewed as two interpenetrating ferromagnetic lattices, at least for $\delta = 0$. This picture is easy to visualize in mean field theory in which the effective field at the 'a' sublattice, say, is determined by two distinct interaction energies J_{aa} and J_{ab} in addition to the local

field h_a [21].

Having split the problem in terms of two sublattices it is possible to view the Kawasaki spin exchange as two composite Glauber processes, one for each sublattice [35]. We may then write down for each sublattice 'a' and 'b' the Glauber rate laws as [36],

$$\dot{m}_a(r,t) = -\frac{1}{\tau}\Big[m_a(r,t) - \tanh\Big\{\beta\Big(\sum_{r,r'}\Big(\sum_{\nu=a,b} J_{a\nu}(r-r')m_\nu(r',t) + h_a(r)\Big)\Big)\Big\}\Big], \quad (3.2.1)$$

and

$$\dot{m}_b(r,t) = -\frac{1}{\tau}\Big[m_b(r,t) - \tanh\Big\{\beta\Big(\sum_{r,r'}\Big(\sum_{\nu=a,b} J_{b\nu}(r-r')m_\nu(r',t) + h_b(r)\Big)\Big)\Big\}\Big], \quad (3.2.2)$$

where τ sets the basic time scale of the Glauber process. Assuming that we are in the *"disordered"* (tetragonal) phase, we may linearize the above equations (3.2.1) and (3.2.2) as

$$\dot{m}_a(r,t) \simeq -\frac{1}{\tau}\Big[m_a(r,t) - \beta\Big(\sum_{r,r'}\Big(\sum_{\nu=a,b} J_{a\nu}(r-r')m_\nu(r',t) + h_a(r)\Big)\Big)\Big], \quad (3.2.3)$$

and similarly

$$\dot{m}_b(r,t) \simeq -\frac{1}{\tau}\Big[m_b(r,t) - \beta\Big(\sum_{r,r'}\Big(\sum_{\nu=a,b} J_{b\nu}(r-r')m_\nu(r',t) + h_b(r)\Big)\Big)\Big]. \quad (3.2.4)$$

The Fourier transform of the equations (3.2.3) and (3.2.4) gives us

$$\dot{m}_a(q,t) \simeq -\frac{1}{\tau}\Big[m_a(q,t) - \beta\Big(\sum_{\nu=a,b} J_{a\nu}(q)m_\nu(q,t) + h_a(q)\Big)\Big], \quad (3.2.5)$$

$$\dot{m}_b(q,t) \simeq -\frac{1}{\tau}\Big[m_b(q,t) - \beta\Big(\sum_{\nu=a,b} J_{b\nu}(q)m_\nu(q,t) + h_b(q)\Big)\Big], \quad (3.2.6)$$

respectively which may now be applied to study the relaxational behavior of the system.

3.3 Anelastic Relaxation

The interstitial oxygen atoms are centers of strain in the host lattice. Accordingly if a uniaxial stress is applied, it will influence the diffusive motion of atoms to the neighboring vacant sites. This elastic diffusion, which occurs due to a gradient in the dilation or contraction results in diffusion relaxation and anelastic strain, known as the Grosky effect [19]. When diffusion processes take place with accompanying reorientation of the elastic dipoles over a picosecond time scale, the resultant reorientation relaxation is known as the Snoek effect, which occurs even under the presence of homogeneous stresses. In the unstressed crystal, and in the tetragonal phase, there is no preferential occupation of the interstitial sites, but when a uniaxial stress is applied, the occupation of 'b' sublattice increases. The consequence of this preferential occupation is the elongation of the crystal along the direction of the applied stress, with a matching contraction in the other direction. Our aim is to study these effects as we approach from above the temperature at which the transition from the tetragonal to the orthorhombic phase takes place. The anelastic relaxation is a time dependent process in which the strain is coupled to particle diffusion.

The quantity of central importance in the experimental study of anelastic relaxation is the frequency dependent compliance $\chi(r,\omega)$ which is a measure of the strain response to an oscillatory external inhomogeneous stress. One of the powerful results of the linear response theory is that $\chi(r,\omega)$ can be obtained directly from the strain response to a time-independent stress using the relaxation-response relation [29]. We have the relation

$$\chi_{\mu\nu\alpha\beta}(r,\omega) = \lim_{z\to -i\omega}\Big[z\tilde{\psi}_{\mu\nu\alpha\beta}(r,z)\Big], \tag{3.3.1}$$

where 'z' is the Laplace transformation variable and $\tilde{\psi}_{\mu\nu\alpha\beta}(r,z)$ is the Laplace transform of the so-called response function, defined by

$$\langle\hat{\varepsilon}_{\mu\nu}(r,t)\rangle = \int dr'\psi_{\mu\nu\gamma\delta}(r-r',t)\sigma_{\gamma\delta}(r'),$$

here we have adopted the usual convention of summation over repeated Greek indices. We want to rewrite the expression for $\langle\hat{\varepsilon}_{\mu\nu}(r,t)\rangle$ in terms of the sublattice magnetization m_a and m_b. Taking the Laplace transform of equation (3.2.5) with respect to time i.e.,

$$L\Big\{F(t)\Big\} = f(z) = \lim_{a\to\infty}\int_0^a e^{-zt}F(t)dt \text{ and } L\Big\{F'(t)\Big\} = zL\Big\{F(t)\Big\} - F(0).$$

Using the above two properties and the linear property of Laplace we get

$$L\Big\{\dot{m}_a(q,t)\Big\} = L\Big\{-\frac{1}{\tau}\Big[m_a(q,t) - \beta\Big(\sum_{\nu=a,b} J_{a\nu}(q)m_\nu(q,t) + h_a(q)\Big)\Big]\Big\}. \tag{3.3.2}$$

From this we get

$$zm_a(q,z) - m_a(q,0) = -\frac{1}{\tau}\Big[m_a(q,z) - \beta\Big(\sum_{\nu=a,b} J_{a\nu}(q)m_\nu(q,z) + z^{-1}h_a(q)\Big)\Big] \tag{3.3.3}$$

where $m_a(q,z)$ is the Laplace transform of $m_a(q,t)$. At time t=0 the external stress is switched on when the system is in the tetragonal phase which is paramagnetic corresponding to $\langle\hat{S}\rangle = 0$ (complete disorder). Therefore, the initial conditions are

$$m_a(q,0) = m_b(q,0) = 0,$$

$$zm_a(q,z) = -\frac{1}{\tau}\Big[m_a(q,z) - \beta\Big(\sum_{\nu=a,b} J_{a\nu}(q)m_\nu(q,z) + z^{-1}h_a(q)\Big)\Big]. \tag{3.3.4}$$

Similarly

$$zm_b(q,z) = -\frac{1}{\tau}\Big[m_b(q,z) - \beta\Big(\sum_{\nu=a,b} J_{b\nu}(q)m_\nu(q,z) + z^{-1}h_b(q)\Big)\Big]. \tag{3.3.5}$$

The stress tensor in terms of the strain tensor can be written as

$$\sigma_{\mu\nu}(q) = L_{\mu\nu\alpha\beta}(q,z)\langle\hat{\varepsilon}_{\alpha\beta}(q,z)\rangle, \tag{3.3.6}$$

where $L_{\mu\nu\alpha\beta}(q,z)$ is the *"elastic modulus tensor"*. Since the applied stress is uniaxial and along the 'y' direction of the rectangular sample, $\mu = \nu = y$ and $\alpha = \beta = x$ *or* y, we have the components of strain along 'x' and 'y' directions only. Denoting $L_{yyxx}(q,z) = \lambda^{(1)}(q,z)$ and $L_{yyyy}(q,z) = \lambda^{(2)}(q,z)$ we obtain then

$$\sigma_{yy}(q) = \lambda^{(1)}(q,z)\langle\hat{\varepsilon}_{xx}(q,z)\rangle + \lambda^{(2)}(q,z)\langle\hat{\varepsilon}_{yy}(q,z)\rangle \tag{3.3.7}$$

the converse relation to equation (3.3.6) is the one in which the strain tensor is written in terms of the stress tensor as

$$\hat{\varepsilon}_{\mu\nu}(q,z) = \tilde{\psi}_{\mu\nu\alpha\beta}(q,z)\langle\sigma_{\alpha\beta}(q)\rangle \tag{3.3.8}$$

where $\tilde{\psi}_{\mu\nu\alpha\beta}(q,z)$, the Fourier-Laplace transform of $\tilde{\psi}_{\mu\nu\alpha\beta}(r,t)$, is called the *"compliance tensor"* with

$$\hat{L}\hat{\tilde{\psi}} = 1,$$

In order to obtain the expression for the modulus first let us rewrite equations (3.3.4) and (3.3.5)as,

$$zm_a(q,z) = -\frac{1}{\tau}\Big[m_a(q,z) - \beta\Big(J_{aa}(q)m_a(q,z) + J_{ab}(q)m_b(q,z)\Big) - \beta z^{-1}h_a(q)\Big], \tag{3.3.9}$$

and

$$zm_b(q,z) = -\frac{1}{\tau}\Big[m_b(q,z) - \beta\Big(J_{ab}(q)m_a(q,z) + J_{bb}(q)m_b(q,z)\Big) - \beta z^{-1}h_b(q)\Big]. \tag{3.3.10}$$

Let us now find $m_b(q,z)$ in terms of $m_a(q,z)$ from equation (3.3.10) we get

$$m_b(q,z) = \frac{\beta J_{ba}(q)}{1+\tau z - \beta J_{bb}(q)}m_a(q,z) + \frac{\beta h_b(q)}{z(1+\tau z - \beta J_{bb}(q))}. \tag{3.3.11}$$

Introducing the time dependence in equations (2.3.12) and (2.3.13) and taking the Laplace transform and from $m_a(q,z) = \langle \hat{S}_a(q,z) \rangle$ and $m_b(q,z) = \langle \hat{S}_b(q,z) \rangle$ we obtain

$$m_a(q,z) = \frac{a_0}{2G_q}\Big[\langle \hat{\varepsilon}_{xx}(q,z)\rangle A_q + \langle \hat{\varepsilon}_{yy}(q,z)\rangle C_q\Big] \tag{3.3.12}$$

and

$$m_b(q,z) = \frac{a_0}{2F_q}\Big[\langle \hat{\varepsilon}_{xx}(q,z)\rangle C_q + \langle \hat{\varepsilon}_{yy}(q,z)\rangle B_q\Big]. \tag{3.3.13}$$

Now substituting equation (3.3.11) in equation (3.3.9) we get

$$\begin{aligned} m_a(q,z)\big[1+\tau z - \beta J_{aa}(q)\big] &= \beta J_{ab}(q)\Big[\frac{\beta J_{ba}(q)}{1+\tau z-\beta J_{bb}(q)} m_a(q,z) \\ &+ \frac{\beta h_b(q)}{z(1+\tau z-\beta J_{bb}(q))}\Big] + \frac{\beta h_a(q)}{z}. \end{aligned} \tag{3.3.14}$$

Now taking m_a two one side we get

$$m_a(q,z)\big[1+\tau z-\beta J_{aa}(q) - \frac{\beta^2 J_{ab}(q)J_{ba}(q)}{1+\tau z-\beta J_{bb}(q)}\big] = \frac{\beta^2 J_{ab}(q)h_b(q)}{z(1+\tau z-\beta J_{bb}(q))} + \frac{\beta h_a(q)}{z}. \tag{3.3.15}$$

Rearranging the above we get

$$\begin{aligned} z m_a(q,z)\big[(1+\tau z)^2 &- \beta(1+\tau z)\{J_{aa}(q)+J_{bb}(q)\} + \beta^2 J_{aa}(q)J_{bb}(q)\big] \\ &= \beta^2\big[J_{ab}(q)h_b(q) - J_{bb}(q)h_a(q)\big] + \beta(1+\tau z)h_a(q). \end{aligned} \tag{3.3.16}$$

Let now substituting the values for $J_{aa}, J_{bb}, J_{ab}, J_{ba}$ from equation (2.2.14) and $m_a(q,z)$ from equation (3.3.12) and

$$h_a(q) = \frac{2\Lambda C_q G_q^*}{a_0(A_qB_q - C_q^2)}\sigma_{yy} \text{ and } h_b(q) = -\frac{2\Lambda A_q F_q^*}{a_0(A_qB_q - C_q^2)}\sigma_{yy}.$$

Then we get

$$\begin{aligned} z m_a(q,z)\Big[(1+\tau z)^2(A_qB_q - C_q^2) &- \beta(1+\tau z)(B_q|G_q|^2 + A_q|F_q|^2) + \beta^2|G_q|^2|F_q|^2\Big] \\ &= \frac{2\Lambda\beta(1+\tau z)C_qG_q^*}{a_0}\sigma_{yy}(q). \end{aligned} \tag{3.3.17}$$

Finally

$$\sigma_{yy}(q) = \frac{za_0^2}{4\Lambda}\beta(1+\tau z)C_q\left|G_q\right|^2\Big[\langle\hat{\varepsilon}_{xx}(q,z)\rangle A_q + \langle\hat{\varepsilon}_{yy}(q,z)\rangle C_q\Big] \quad (3.3.18)$$
$$\times \Big[(1+\tau z)^2(A_qB_q - C_q^2) - \beta(1+\tau z)(B_q\left|G_q\right|^2 + A_q\left|F_q\right|^2) + \beta^2\left|G_q\right|^2\left|F_q\right|^2\Big],$$

we get finally the expression for $\sigma_{yy}(q)$ in terms of $\langle\hat{\varepsilon}_{xx}\rangle, \langle\hat{\varepsilon}_{xx}\rangle$ and all other basic microscopic parameters of the model. Comparing the expression of $\sigma_{yy}(q)$ with equation (3.3.7) we note that the elastic modulus for $\lambda^{(1)}(q,z)$ and $\lambda^{(2)}(q,z)$ becomes

$$\lambda^{(1)}(q,z) = \frac{za_0^2A_q\Big[(1+\tau z)^2(A_qB_q - C_q^2) - \beta(1+\tau z)(B_q\left|G_q\right|^2 + A_q\left|F_q\right|^2) + \beta^2\left|G_q\right|^2\left|F_q\right|^2\Big]}{4\Lambda\beta(1+\tau z)C_q\left|G_q\right|^2} \quad (3.3.19)$$

and

$$\lambda^{(2)}(q,z) = \frac{za_0^2C_q\Big[(1+\tau z)^2(A_qB_q - C_q^2) - \beta(1+\tau z)(B_q\left|G_q\right|^2 + A_q\left|F_q\right|^2) + \beta^2\left|G_q\right|^2\left|F_q\right|^2\Big]}{4\Lambda\beta(1+\tau z)C_q\left|G_q\right|^2}. \quad (3.3.20)$$

Inverting the expressions for $\lambda^{(1)}(q,z)$ and $\lambda^{(2)}(q,z)$ we get the corresponding expressions for the response function $\psi^{(1)}(q,z)$ and $\psi^{(2)}(q,z)$ respectively, where $\tilde{\psi}_{yyxx}(q,z) = \psi^{(1)}(q,z)$ and $\tilde{\psi}_{yyyy}(q,z) = \psi^{(2)}(q,z)$. Thus

$$\psi^{(2)}(q,z) = \frac{4\Lambda\beta(1+\tau z)\left|G_q\right|^2}{za_0^2\Big[(1+\tau z)^2(A_qB_q - C_q^2) - \beta(1+\tau z)(B_q\left|G_q\right|^2 + A_q\left|F_q\right|^2) + \beta^2\left|G_q\right|^2\left|F_q\right|^2\Big]}. \quad (3.3.21)$$

Similarly we can get the expression for $\psi^{(1)}(q,z)$ from equation (3.3.19) by inverting the expression for $\lambda^{(1)}(q,z)$. The expression for the frequency dependent compliance is obtained from equation (3.3.21) (neglecting terms of order of β^2) and using equation (3.3.1) when the transition temperature is approached from the disordered phase. Thus we have

$$\psi^{(2)}(q,z) \simeq \frac{4\Lambda\beta\left|G_q\right|^2}{za_0^2\Big[(1+\tau z)(A_qB_q - C_q^2) - \beta(B_q\left|G_q\right|^2 + A_q\left|F_q\right|^2)\Big]}. \quad (3.3.22)$$

By introduce the above equation (3.3.22) in equation (3.3.23) i.e.,

$$\chi^{(2)}(q,\omega) = \lim_{z\to -i\omega}\Big[z\psi^{(2)}(q,z)\Big] \tag{3.3.23}$$

we get

$$\chi^{(2)}(q,\omega) = \frac{4\Lambda\beta\left|G_q\right|^2}{a_0^2\Big[(1-i\tau\omega)(A_qB_q-C_q^2)-\beta(B_q\left|G_q\right|^2+A_q\left|F_q\right|^2)\Big]}. \tag{3.3.24}$$

Let us simplify this to bring in Curie-Weiss form

$$\begin{aligned}
\chi^{(2)}(q,\omega) &= \frac{4\Lambda\beta\left|G_q\right|^2}{a_0^2(A_qB_q-C_q^2)\Big[(1-\tau i\omega)-\frac{\beta(B_q|G_q|^2+A_q|F_q|^2)}{(A_qB_q-C_q^2)}\Big]} \\
&= \frac{4\Lambda\beta\left|G_q\right|^2\Big/a_0^2(A_qB_q-C_q^2)}{\big[(1-i\tau\omega)-\beta J_q\big]} \\
&= \frac{4\Lambda\beta\left|G_q\right|^2\Big/a_0^2(A_qB_q-C_q^2)}{\big[(1-\beta J_q)-i\tau\omega\big]} \\
&= \frac{4\Lambda\beta\left|G_q\right|^2\Big/a_0^2(A_qB_q-C_q^2)}{(1-\beta J_q)\big[1-\frac{i\tau\omega}{(1-\beta J_q)}\big]}.
\end{aligned} \tag{3.3.25}$$

Finally we get

$$\chi^{(2)}(q,\omega) = \frac{4\Lambda\beta\left|G_q\right|^2\Big/a_0^2(A_qB_q-C_q^2)}{\big[1-\beta J_q\big]\big[1-i\omega\tau_q\big]} \tag{3.3.26}$$

where the relaxation time τ_q and the interaction energy J_q are defined as

$$\tau_q = \frac{\tau}{1-\beta J_q},$$

and

$$J_q = \frac{B_q\left|G_q\right|^2+A_q\left|F_q\right|^2}{A_qB_q-C_q^2}.$$

Therefore, relaxation time associated with every 'q' mode diverges when the ferroelastic transition temperature is approached, i.e., when

$$\beta J_q = 1.$$

As discussed in chapter two, a by-product of equation (3.3.26) is an expression for the transition temperature T_s, given by

$$T_s = \lim_{q\to 0} \frac{B_q \left|G_q\right|^2 + A_q \left|F_q\right|^2}{k_B\big(A_q B_q - C_q^2\big)}. \tag{3.3.27}$$

Expanding the expressions in equation (2.2.5) until second order and neglecting higher orders from A_q to G_q for small 'q' i.e.,

$$\begin{aligned} A_q &\simeq \frac{a_0^2 q_x^2}{2}(K+K') + \frac{a_0^2 q_y^2}{2}(K') \\ B_q &\simeq \frac{a_0^2 q_y^2}{2}(K+K') + \frac{a_0^2 q_x^2}{2}(K') \\ C_q &\simeq a_0^2 q_x q_y K' \\ F_q &\simeq i\frac{\alpha a_0 q_y}{2}K \\ G_q &\simeq i\frac{\alpha a_0 q_x}{2}K. \end{aligned} \tag{3.3.28}$$

Inserting the above equation (3.3.28) in $B_q \left|G_q\right|^2 + A_q \left|F_q\right|^2$ we get

$$B_q \left|G_q\right|^2 + A_q \left|F_q\right|^2 \simeq \frac{\alpha^2 a_0^4 q_x^2 q_y^2}{4}(K^2(K+K')) \tag{3.3.29}$$

and

$$A_q B_q - C_q^2 \simeq \frac{a_0^4 q_x^2 q_y^2}{4}(K^2 + 2K'(K-K')). \tag{3.3.30}$$

Substituting equation (3.3.29) and (3.3.30) in equation (3.3.27) we get

$$T_s \simeq \frac{\alpha^2 K^2 (K+K')}{k_B(K^2 + 2K'(K-K'))} \tag{3.3.31}$$

which is the ferroelastic transition temperature at which the internal friction (to an applied inhomogeneous stress) diverges. Note that T_s is completely determined by the basics parameters of the Spring-Defect model.

The internal friction or the loss tangent can now be readily obtained from equation (3.3.26) using the relation

$$\tan\phi(\omega) = \chi_u^{-1}\,\mathrm{Im}\,\chi(0,\omega). \tag{3.3.32}$$

$$\begin{aligned}
\mathrm{Im}\,\chi^{(2)}(q,\omega) &= \mathrm{Im}\left(\frac{4\Lambda\beta\,|G_q|^2\Big/a_0^2(A_qB_q - C_q^2)}{\big[1-\beta J_q\big]\big[1-i\omega\tau_q\big]}\right)\\
&= \mathrm{Im}\left(\frac{4\Lambda\beta\,|G_q|^2\Big/a_0^2(A_qB_q - C_q^2)}{\big[1-\beta J_q\big]\big[1-i\omega\tau_q\big]}\frac{\big[1+i\omega\tau_q\big]}{\big[1+i\omega\tau_q\big]}\right)\\
&= \mathrm{Im}\left(\frac{4\Lambda\beta\,|G_q|^2\Big/a_0^2(A_qB_q - C_q^2)}{\big[1-\beta J_q\big]\big[1+\omega^2\tau_q^2\big]}\big[1+i\omega\tau_q\big]\right)\\
&= \frac{4\Lambda\beta\,|G_q|^2\Big/a_0^2(A_qB_q - C_q^2)}{\big[1-\beta J_q\big]\big[1+\omega^2\tau_q^2\big]}\big[\omega\tau_q\big]
\end{aligned} \tag{3.3.33}$$

where χ_u is the (unrelaxed) elastic modulus of the host material. We present numerical results for the internal friction in fig. (3.1). In the high temperature limit (highly disordered phase) and for $\omega = 0$ (static case) the above expression equation (3.3.26) reduces to the expected Curie form (see also chapter two equation (2.4.29)) i.e.,

$$\chi^{(2)}(q,0) \simeq \frac{4\Lambda\beta\,|G_q|^2}{a_0^2\Big[(A_qB_q - C_q^2)\Big]}. \tag{3.3.34}$$

The expected Curie-Weiss-Ornstein-Zernicke form of the static compliance is recovered from equation (3.3.26) (by neglecting terms of order β^2). When the transition temperature is approached from the disordered phase (see also chapter two equation (2.4.31)) we get,

$$\chi^{(2)}(q) \simeq \frac{4\Lambda\,|G_q|^2\Big/a_0^2k_B(A_qB_q - C_q^2)}{\Big(T - \frac{B_q|G_q|^2 + A_q|F_q|^2}{k_B(A_qB_q - C_q^2)}\Big)}. \tag{3.3.35}$$

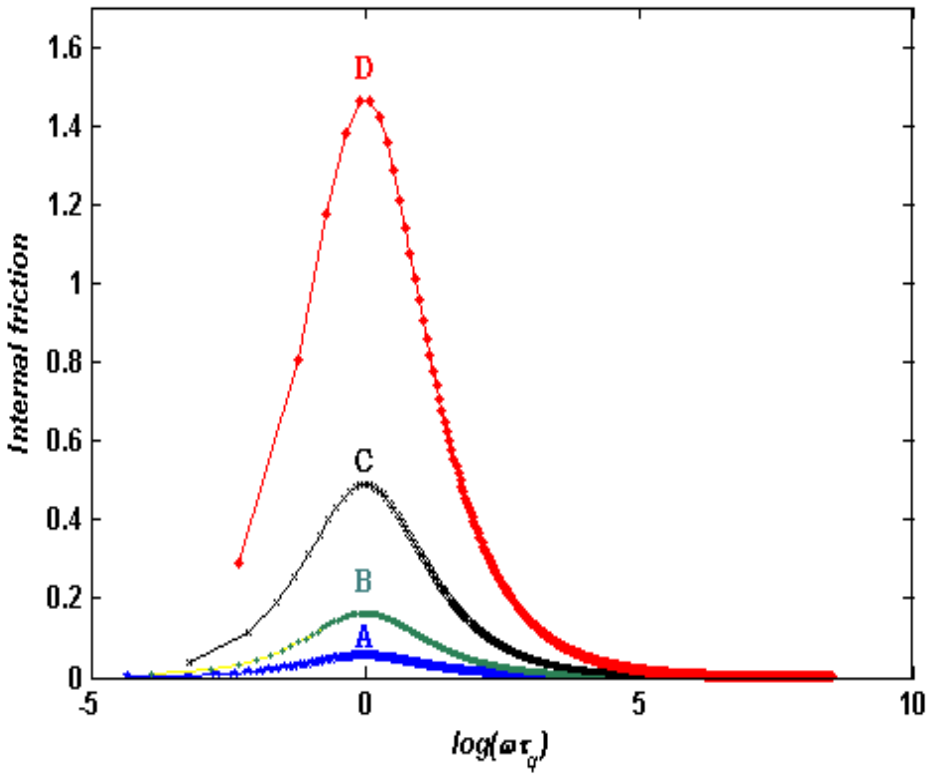

Figure 3.1: *The internal friction, versus* $log(\omega\tau_q)$*, for different values of* $\varphi = T_s/T$*: curve A,* φ*=0.25; curve B,* φ*=0.5; curve C,* φ*=0.75, curve D,* φ*=0.9. It can be seen that as T approaches the phase transformation point* (T_s)*(i.e.,*φ *increases, the internal friction becomes sharp and broad.*

The Curie-Weiss law for the static compliance as well as the frequency dependent compliance as the system develops a spontaneous strain while undergoing a transition from the high temperature tetragonal phase to the low temperature orthorhombic phase, is similar to the one derived by Wadhawan et al, 1991. However, they have only dealt with the static case, whereas we have presented both static and the dynamic results. There are other important differences between our approach and that

of Wadhawan et al, 1991. While both approaches are based on the fact that the structural transition and the concomitant ferroelasticity in YBCO are driven by loosely bound oxygen interstitial atoms in the Cu-O plane, our method relies on a fully statistical mechanical treatment of a microscopic Hamiltonian. Further, our theory has a unique transition temperature T_s which characterizes the tetragonal to orthorhombic transformation as well as the paraelastic to ferroelastic transition, in contrast to two different transition temperature that appear in the work of Wadhawan et al, which they associate with Snoek and Grosky processes.

Chapter 4

Results and Discussion

In chapter two we have considered the spontaneous development of strain as the system undergoes structural transition from the tetragonal to the orthorhombic phase, from microscopic considerations. As mentioned earlier, the present treatment is valid only for $\delta = 0$. For $\delta \neq 0$ complex orderings are possible which are not included in our simple minded model [23, 24]. It has been shown that the interaction between the strain fields around interstitial oxygen defects favors a situation in which the oxygen atoms preferentially occupy one of the two possible sublattices in the tetragonal phase. A straight forward mean-field theory yields a *Staggered magnetization* which is the relevant order parameter. The temperature dependence of the order parameter shows that the long ranged strain induced coupling between the defects induces a second order phase transition from tetragonal to the orthorhombic phase. The MFA also provides a qualitative estimate of the transition temperature (T_s) in terms of the microscopic parameters of the basic spring-defect model, introduced by us earlier [16].

We have also addressed the question of studying the tetragonal to orthorhombic

transformation as modeled above, by the experimental technique of internal friction which measures, amongst other things, the compliance i,e., the static response of the system to an applied stress [25]. The calculated compliance $\chi^{(i)}_{(r)}$ follows the expected Curie-Weiss behavior. The question of kinetics is also of great importance, especially in relation to the hopping diffusion of oxygen in YBCO. As the oxygen jumps into the neighboring site the associated Zener dipole flips its orientation, leading to anelastic relaxation [19]. At the microscopic level each flip of the Zener dipole is linked with an exchange of sites by an oxygen-vacancy pair, which in the Ising language, can be described by a Kawasaki process [26]. Thus all relaxational characteristics associated with frequency-dependent compliance, internal friction, etc., can be studied by means of the Kawasaki model. These issues related to kinetics was discussed in chapter three.

In chapter three Our principal aim was to study the diffusive behavior of the interacting interstitial oxygen defects in YBCO and the associated anelastic relaxation. We made use of a mean field approach (MFA) based on Glauber spin flip in each sublattice of an antiferromagnetically coupled system, which is approximately equivalent to the Kawasaki spin exchange that describes the hopping of the oxygen atoms from one site to another. The internal friction is derived in terms of basic parameters such as K, K' and α. The internal friction peak based on equation (3.3.32) is plotted for different T_s/T. The four curves in fig.(3.1) correspond to four different values of T_s/T. We observe that as T_s/T increases, the curves shows a broadening and an increase in height of the peak. These features are in qualitative agreement with the experimental findings of Zhang et al, 1990 on single phase YBCO specimen. As T approaches T_s from the disorder state the response (which is the internal friction)

increases. It can be seen that as T approaches the structural transition temperature (T_s) the peak becomes sharp. The plot of internal friction has been shown to exhibit a broadening of the peak as the transition temperature is approached from above in the disordered phase.

The MFA is expected to yield a qualitatively correct estimate of the transition temperature (T_s) in terms of certain basic parameters of the model which is presented in equation (2.4.32). In the present order-disorder case, however, the appropriate order parameter (staggered magnetization) is not conserved during a Kawasaki process. Its time dependence is therefore treated through the Glauber master equation. The latter, in mean field theory, yields a rate equation for the magnetization, which has been used for calculating the creep function (response function) near the phase transition point. It is evident that the system has viscoelastic -like properties as a consequence of the slowing down of the relaxation near the ferroelastic phase transition [22].

Bibliography

[1] J. G. Bednorz and K. A. Müller, z. Phys. B **64**, 189 (1986).

[2] M. K. Wu, J. R. Ashburn, C. J. Torng, P. H. Hor, R. L. Meng, L. Gao, Z. J. Huang, Y. Q. Wang and C. W. Chu, Phys. Rev. Lett. **58**, 908 (1987).

[3] http://www.superconductors.org/History.htm, (2007)

[4] V. Arkadiev, *Superconductivity defeats gravity*, Nature **160**, 330 (1947).

[5] J. Emanuelson, *An introduction to the new oxide superconductors*, Colorado Futurescience Inc., (1989).

[6] T. P. Sheahen, *Introduction to High-Temperature Superconductivity*, Springer, (2002).

[7] *Introduction to $YBa_2Cu_3O_x$ Superconductor*, Critical Review and Technology Assessment, (2002).

[8] W. Meissner and R. Ochsenfeld, Naturwiss **21**, 787 (1933).

[9] J. D. Jorgensen, B. W. Veal, A. P. Paulikas, L. J. Nowicki, G. W. Crabtree, H. Claus and W. K. Kwok, Phys. Rev. B **41**, 1863 (1990).

[10] http://aiff.usc.es/ mclbt/teresa/YBCO.html, (2004).

[11] T. Silver, A. V. Pan, M. Ionescu, M. J. Qin and S. X. Dou *Developments in high temperature superconductivity*, Annu. Rep. Prog. Chem., Sect. C **98**, 323 (2002).

[12] D. R. Graves, MSEE and PE, *Introduction to High Temperature Superconductors*, (1994).

[13] Robert W. Dull, *A Teacher's Guide to Superconductivity for High School Students*, (1994).

[14] Ekhard K. H. Salje, Stuart A. Haywarda and William T. Lee, *Ferroelastic phase transitions: structure and micro- structure*, Acta Cryst. A **61**, 3 (2005).

[15] Gebeyehu Tadesse, M.Sc. Thesis, *A microscopic model for structural phase transition of YBCO*, Addis Ababa University, Department of Physics, (2007).

[16] S. Dattagupta, S. K. Ghoshal, *Spring-Defect Model of Structural Phase Transition in YBCO*, Sol. St. Comm. **88**, 547 (1993).

[17] C. Zener, *Elasticity and Anelasticity of Metals*, University of Chicago Press, Chicago, Illinois, 125 (1948).

[18] S. K. Ghoshal and S. Dattagupta, *3-d Model for strain ordering in steel II: Relaxation effects*, Pramana **51**, 539 (1998).

[19] A. S. Nowick and B. S. Berry, *Anelastic Relaxation in Crystalline Solids*, Academic Press, New York, (1972).

[20] E. D. Landau and E. M. Lifshitz, *Theory of Elasticity*, Pergamon Press, (1986).

[21] J. S. Smart, *Effective Field Theories of Magnetism*, Academic press, (1963)

[22] S. Dattagupta, R. Balakrishnan and R. Ranganathan, J. Phys. F: Met. Phys. **12**, 1345 (1982).

[23] V. K. Wadhawan, *The role of basal-plane oxygen atoms in determining the ferroelastiv and microstructural properties of Y-Ba-Cu-O*, Bull. Mater. Sci. **14**, 561 (1991).

[24] A. G. Khachaturyan and J. W. Morris, Jr., *Ordering and Decomposition in the High-Temperature Superconducting Compound* $YBa_2Cu_3O_x$, Phys. Rev. Lett. **59**, 2776 (1987).

[25] J. X. Zhang, G. M. Lin, W. G. Zeng, K. F. Liang, Z. C. Lin, G. G. Siu, M. J. Stokes and P. C. W. Fung, *Superconductor Science and Technology*, **3**, 113 (1990).

[26] K. Kawasaki, Phys. Rev. **145**, 224 (1966).

[27] S. A. Gridnev and O. N. Ivanov, *The influence of ferroelastic twins on the properties of superconducting* $YBa_2Cu_3O_{7-\delta}$ *ceramics*, Ferroelectrics **128**, 185 (1992).

[28] S. K. Ghoshal and S. Dattagupta, *3-d Model for strain ordering in steel I: Static effects*, Pramana **51**, 519 (1998).

[29] V. Balakrishnan, S. Dattagupta and G. Venkataraman, *A stochastic theory of anelastic creep*, Philosophical Magazine A **37**, 65 (1978).

[30] M. Sarikaya, E. A. Stern, *Local structural variations in* $YBa_2Cu_3O_{7-x}$, Phys. Rev. B **37**, 9373 (1988).

[31] G. Cannelli, R. Cantelli, F. Cordero, *New anelastic relaxation effect in Y-Ba-Cu-O at low temperature: A Snoek-type peak due to oxygen diffusion*, Phys. Rev. B **38**, 7200 (1988).

[32] Simon Marais, Volker Heine, Chris Nex, and Ekhard Salje, *Phenomena due to strain coupling in phase transitions*, Phys. Rev. Lett. **66**, 2480 (1991).

[33] J. Dominec, *Sound attenuation and velocity in superconductive ceramics-a review*, Supercond. Sci. Technol. **2**, 91 (1989).

[34] E. Bonetti, E. G. Campari, P. Cammarota, A. Casagrande and S. Mantovani, *Dynamic Youngs modulus relaxation and softening in* $YBa_2Cu_3O_{7-x}$, Supercond. Sci. Technol. **4**, 196 (1991).

[35] R. J. Glauber, *Time-dependent statistics. of the Ising model.*, J. Math. Phys. **4**, 294 (1963).

[36] M. Suzuki and R. Kubo, *Dynamics of the Ising Model near the Critical Point-I*, J. Phys. Soc. Jpn. **24**, 51 (1968).

DECLARATION

I here by declare that this thesis has been presented with the help of my advisor as well as my instructor and has not been presented for a degree in any other university. All sources of material used for the thesis have been duly acknowledged.

Name: Ashenafi Weldemariam

Signature: .....

This thesis has been submitted for the examination with my approval as university advisor.

Name: Dr. S. K. Ghoshal

Signature: .....

Addis Ababa University
Department of Physics
August 2007